

1 **Field-scale CH₄ emission at a sub-arctic mire with heterogeneous permafrost thaw status**

2 Patryk Łakomic¹, Jutta Holst¹, Thomas Friborg², Patrick Crill³, Niklas Rakos⁴, Natascha Kljun⁵, Per-
3 Ola Olsson¹, Lars Eklundh¹, Andreas Persson¹, Janne Rinne¹

4 ¹ Department of Physical Geography and Ecosystem Science, Lund University, 223 62, Sweden

5 ² Department of Geosciences and Natural Resource Management, University of Copenhagen,
6 1165, Denmark

7 ³ Department of Geological Sciences and Bolin Centre for Climate Research, Stockholm
8 University, 114 19, Sweden

9 ⁴ Abisko Scientific Research Station, Swedish Polar Research Secretariat, Abisko, 981 07, Sweden

10 ⁵ Centre for Environmental and Climate Science, Lund University, 223 62, Sweden

11

12 *Correspondence to:* Patryk Łakomic (patryk.lakomic@nateko.lu.se)

13

14 **Abstract**

15 The Arctic is exposed to even faster temperature changes than most other areas on Earth.
16 Constantly increasing temperature will lead to thawing permafrost and changes in the methane
17 (CH₄) emissions from wetlands. One of the places exposed to those changes is the Abisko-
18 Stordalen Mire in northern Sweden, where climate and vegetation studies have been conducted
19 since the 1970s.

20 In our study, we analyzed field-scale methane emissions measured by the eddy covariance
21 method at Abisko-Stordalen Mire for three years (2014-2016). The site is a subarctic mire mosaic
22 of palsas, thawing palsas, fully thawed fens, and open water bodies. A bimodal wind pattern
23 prevalent at the site provides an ideal opportunity to measure mire patches with different
24 permafrost status with one flux measurement system. The flux footprint for westerly winds is
25 dominated by elevated palsa plateaus, while the footprint is almost equally distributed between
26 palsas and thawing bog-like areas for easterly winds. As these patches are exposed to the same
27 climatic and weather conditions, we analyzed the differences in the responses of their methane
28 emission for environmental parameters.

29 The methane fluxes followed a similar annual cycle over the three study years, with a gentle rise
30 during spring and a decrease during autumn, without emission burst at either end of the ice-free
31 season. The peak emission during the ice-free season differed significantly for the mire with two
32 permafrost status: the palsa mire emitted 19 mg-C m⁻² d⁻¹ and the thawing wet sector 40 mg-C m⁻²
33 d⁻¹. Factors controlling the methane emission were analyzed using generalized linear models.
34 The main driver for methane fluxes was peat temperature for both wind sectors. Soil water
35 content above the water table emerged as an explanatory variable for the three years for western
36 sectors and the year 2016 in the eastern sector. The water table level showed a significant

37 correlation with methane emission for the year 2016 as well. Gross primary production, however,
38 did not show a significant correlation with methane emissions.
39 Annual methane emissions were estimated based on four different gap-filing methods. The
40 different methods generally resulted in very similar annual emissions. The mean annual emission
41 based on all models was $3.1 \pm 0.3 \text{ g-C m}^{-2} \text{ a}^{-1}$ for the western sector and $5.5 \pm 0.5 \text{ g-C m}^{-2} \text{ a}^{-1}$ for
42 the eastern sector. The average annual emissions, derived from these data and a footprint
43 climatology, were $2.7 \pm 0.5 \text{ g-C m}^{-2} \text{ a}^{-1}$ and $8.2 \pm 1.5 \text{ g-C m}^{-2} \text{ a}^{-1}$ for the palsa and thawing surfaces,
44 respectively. Winter fluxes were relatively high, contributing 27 - 45 % to the annual emissions.
45

46 1 Introduction

47 After a period of stabilization in the late 1990s to early 2000s, atmospheric methane (CH_4)
48 concentration is increasing again at rates similar to those before 1993, which is approximately
49 12 ppb yr^{-1} (Dlugokencky et al. 2011, Nisbet et al. 2014, Saunois 2020). The reasons behind this
50 increase are still partly unclear, as the mechanisms that control the global CH_4 budget are not
51 completely understood (Kirschke et al. 2013, Saunois et al. 2020). The largest natural source of
52 CH_4 are wetlands, based on top-down emission estimates (Saunois et al. 2020), and this source
53 may become stronger in the warming climate (Zhang et al. 2017). The shift in the isotopic
54 composition of CH_4 towards more negative values also supports the hypothesis of changes in the
55 biological source strength driving the increase in CH_4 concentration, as atmospheric CH_4 is
56 becoming more ^{13}C -depleted (Nisbet et al. 2016).

57 Increasing temperature has shown to speed up the degradation of permafrost which leads to
58 losses in the soil carbon pool, often in the form of carbon dioxide (CO_2) and CH_4 (Malmer et al.
59 2005). The high northern latitudes are experiencing the fastest temperature increase due to the
60 ongoing global warming. Temperature changes in the Arctic have been twice as high as the global
61 average (Post et al. 2019).

62 Ecosystems near the annual near-surface air temperature isotherms of $0 \text{ }^\circ\text{C}$ are vulnerable to
63 permafrost thaw and changes in ecosystem characteristics in a warming climate. These
64 vulnerable ecosystems include palsa mires, such as Stordalen Mire near Abisko, Sweden, where
65 the recent warming has led to annual average temperatures exceeding $0 \text{ }^\circ\text{C}$ since 1980s
66 (Callaghan et al. 2010, Callaghan et al. 2013, Post et al. 2019, Figure S1). The warming has led to
67 an acceleration of permafrost thaw processes and a transition from palsa plateaus, underlain by
68 permafrost, to non-permafrost fen systems (Malmer et al. 2005). These deviations are likely to
69 induce changes in biogeochemical processes, including increased CH_4 emissions (Christensen et
70 al. 2003).

71 The most direct micrometeorological field-scale method used to measure CH_4 exchange between
72 ecosystem and atmosphere is the eddy covariance (EC) method (e.g. Verma et al. 1986, Aubinet
73 et al., 2012). The advantages of this method are its high temporal resolution and minimal
74 disturbance to the measured surface. Thus, it is feasible for long-term measurements of rates of
75 gas exchange that integrates over surface variation (Knox et al. 2016, Li et al. 2016, Rinne et al.

76 2018). However, information on the small-scale spatial distribution of surface fluxes is lost with
77 the method due to the spatially integrative nature of the EC method. Instead of resolving the
78 small-scale spatial variability, the EC method provides averaged fluxes from a larger area, the flux
79 footprint area (Kljun et al. 2002). However, spatial variability can be resolved by the EC method
80 using measurements conducted under different wind directions, as the footprint area is located
81 upwind of the measurement tower. We can take advantage of this feature to obtain gas exchange
82 rates from two different ecosystem types with one measurement system by placing the
83 measurement system on the border between these systems (e.g. Jackowicz-Korczyński et al.,
84 2010; Kowalska et al., 2013; Jammot et al., 2015; 2017). Stordalen Mire offers an excellent
85 opportunity to conduct flux studies where one flux system is used to monitor two ecosystem
86 types since the wind direction is bimodal. While previous studies in the area have compared open
87 water surfaces to completely thawed fen (Jammot et al., 2015, 2017, Jansen et al. 2020), no
88 comparison of field-scale CH₄ emission between permafrost palsa plateaus and thawing wet
89 areas has been conducted yet.

90 Previous studies on CH₄ emission within the Stordalen Mire from areas with different permafrost
91 status have been done using chamber measurements (McCalley et al. 2014, Deng et al. 2014).
92 McCalley et al. (2014) reported CH₄ emissions from palsas underlain by permafrost to be close to
93 zero, summertime emissions from thawing wet areas to be around 25 mg-C m⁻² d⁻², while
94 completely thawed fen sites revealed much higher emission of 150 mg-C m⁻² d⁻². There are only
95 few wintertime data on CH₄ emission available using the chamber method (Christensen et al.
96 2000, Nilsson et al. 2008, Godin et al. 2012, McCalley et al. 2014). However, EC measurements
97 conducted at different northern mires typically show low but positive emissions in winter (Rinne
98 et al., 2007; Yamulki et al. 2013, and others).

99 In this study we analyzed field-scale CH₄ emission from two areas of Stordalen subarctic mire.
100 The first area is dominated by drained permafrost plateau. The second area is thawing and thus
101 resulting in wetter conditions. Outputs from this analysis are differences in the CH₄ emissions
102 from the mire patches with heterogeneous permafrost status. We are expecting, based on the
103 previous studies, that fluxes from the wetter sector will be around 30 mg-C m⁻² d⁻², while the
104 palsa plateau will emit significantly lower fluxes during the peak season. We presume that
105 winter fluxes will be positive but very low.

106
107 For estimation of annual CH₄ emission we need gap-free datasets. Up to date, there is no
108 generally accepted gap-filling method for CH₄ fluxes, hence four different gap-filling methods
109 were compared. The test of the four methods will decrease the uncertainty in the annual balance
110 estimation (Hommeltenberg et al. (2014), Rößger et al. (2019), Kim et al. (2019)). It was important
111 to use more than one method in this case of study because datasets were portioned and due to
112 that contained more gaps.

113 This study aimed to estimate the annual CH₄ emission from two distinct different ecotypes, with
114 heterogeneous permafrost status, exposed to the same environmental factors. Furthermore, we

115 analyzed the seasonal cycle of CH₄ emission to quantify the contribution during different seasons.
116 Moreover, an analysis of differences in controlling factors for these two different areas was done.
117

118 2 Materials and method

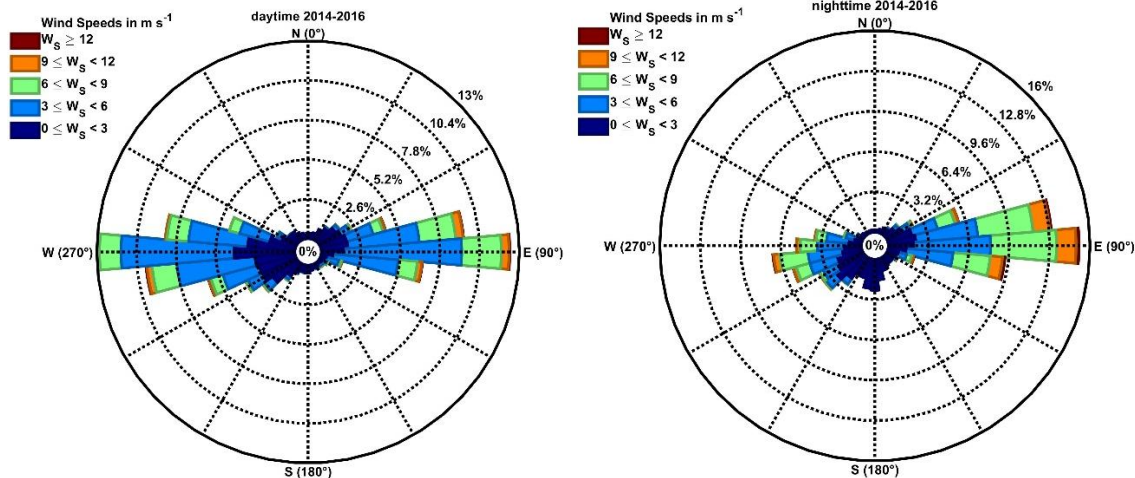
119 2.1 Study site

120 The study area is Stordalen Mire, a mire complex underlain by discontinuous permafrost located
121 in northern subarctic Sweden (68°20' N, 19°30' E) near Abisko (Ábeskovvu). The station Abisko-
122 Stordalen (SE-Sto) is a part of the ICOS Sweden research infrastructure and is the only one in
123 Sweden situated in the subarctic region. The measurement period that is analyzed here covers
124 three years from 2014 to 2016. The mean annual near- surface air temperature in this region has
125 been increasing during the last decades, and temperatures recorded by SMHI (Sveriges
126 meteorologiska och hydrologiska institut) at ANS (Abisko Naturvetenskapliga Station) has
127 exceeded the 0 °C threshold since the late 1980s (Callaghan et al. 2013, Figure S1). During the
128 years 2014-2016, the mean near-surface air temperature (Ta) was 1.0 °C and 0.3 °C at ANS and
129 the ICOS Sweden station Abisko-Stordalen (SE-Sto), respectively. The average annual
130 precipitation, based on ANS data, is around 330 mm yr⁻¹. An acceleration of permafrost loss with
131 increasing temperatures is likely (Callaghan et al. 2013).

132 The large mountain valley of Lake Torneträsk (Duortnosjávri) channels winds at the study site,
133 leading to a bimodal wind distribution (Figure 1), which allows us to divide our analyses into two
134 distinct sectors. The plant community structure around the tower is determined by the hydrology
135 which in turn is determined by the microtopographic variation in the surface due to the local
136 permafrost dynamics. Different plant communities would have different productivities thus
137 controlling the CO₂ and CH₄ fluxes from those surfaces. The area to the west of the EC mast is
138 dominated by a drier permafrost palsa plateau hereafter referred to as the western sector,
139 whereas the area to the east is a mixture of thawing wet areas and palsas, hereafter referred to
140 as the eastern sector. The drained permafrost plateau is dominated by *Empetrum*
141 *hermaphroditum*, *Betula nana*, *Rubus chamaemorus*, *Eriophorum vaginatum*, *Dicranum*
142 *elongatum*, *Sphagnum fuscum*. The wet areas are characterizing by *E. vaginatum*, *Carex*
143 *rotundata*, *S. balticum*, *Drepanucladus schulzei*, *Politrichum jensenii* (Johansson et al. 2006). The
144 thawing areas in this sector exhibit ombrotrophic, bog-like, features. Dominant vegetation varies
145 with the microforms of the mire.

147

148



149

150 Figure 1. The wind rose for SE-Sto tower for years 2014-2016 for the daytime (left panel) and nighttime
 151 (right panel)

152

153

154 2.2 Flux measurements

155 The EC measurements of CH_4 fluxes at SE-Sto are made using a closed-path fast off-axis
 156 integrated cavity output spectrometer (OA-ICOS LGR model GGA-24EP, ABB Ltd, Zurich,
 157 Switzerland) combined with a 3-D sonic anemometer (SA-Metek uSonic-3 CLASS A, Metek GmbH,
 158 Germany). Air was sampled via a 29.6 m long polyethylene tubing with an 8.13 mm inner
 159 diameter. Analysis of the high-frequency loss were performed to assess the effect of relatively
 160 long sample tubing. We analyzed this with the co-spectra of the CH_4 and the vertical wind speed
 161 w . The analysis did not show a dampening effect at the high frequencies (Figure S2), thus the high
 162 frequency attenuation does not seem to be very large. Furthermore, the post-processing
 163 software we used to calculate fluxes includes correction for high-frequency losses. The nominal
 164 tube flow rate was 36 l min^{-1} . The sampling inlet was displaced 22 cm horizontally of the sonic
 165 anemometer measurement volume towards 180° . The response time of the LGR-FGGA was 0.1 s.
 166 The LGR FGGA was placed inside a heated and air-conditioned shelter. The anemometer was
 167 located north of the instrument shelter and was oriented with the sensors north pointing towards
 168 186° . This orientation allows undisturbed wind measurements from both main wind directions,
 169 East and West.

170 CO_2 and H_2O were measured with a LI-COR LI-7200 (LI-COR Environment, USA) closed path infra-
 171 red gas analyzer. The sampling inlet was at the same location as the sampling point for the CH_4
 172 analyzer. Sampled air was transported through 1.05 m and of 5.3 mm ID tubing. The nominal
 173 tube flow rate was 15 l min^{-1} .

174 The anemometer and air sampling tubes were mounted on a mast of 2.2 m above ground level
 175 (a.g.l.) ($68^\circ 21' 21.32'' \text{ N}$, $19^\circ 2' 42.75'' \text{ E}$), placed at the edge of the western and the eastern sectors.

176 Data were collected by an ISDL data logger (In Situ Instrument AB, Sweden) with a 20 Hz time
177 resolution.

178

179 2.3 Ancillary Measurements

180 Ancillary measurements are presented in Table S1. The sampling frequency for these parameters
181 was 1 Hz and the collected data were averaged into half-hourly values. Measured variables are
182 divided into two categories: peat/soil parameters, and meteorological parameters. Peat
183 temperatures at each depth, soil heat fluxes, and soil water contents (SWC) were measured at
184 four locations around the EC tower, located towards the four cardinal directions. In further
185 analysis, data just from two of these locations were used (East and West) as these were within
186 the flux footprint areas of the EC tower. The sites for the water table level (WTL) measurements
187 differed from the peat temperature profiles. The soil pit for temperature and moisture probe in
188 the western sector is located on a palsa plateau. However, the WTL probe is located in a pond
189 approximately 10 m away from the soil temperature and SWC measurement, as there is no WTL
190 above the permafrost of palsas. The soil pit for temperature and SWC probe in the eastern sector
191 is located in the wet thawing area. The WTL probe is located in the wetter area approximately 10
192 m away. Furthermore, data for WTL was available only during the unfrozen period, as the probes
193 were removed during the frozen period to avoid damage. Meteorological variables were
194 measured on a separate mast, placed 10 meters south-west of the flux measurement mast.

195

196 2.4 Flux calculation

197 Fluxes of CO₂, CH₄, H₂O, and sensible heat were calculated using EddyPro 6.2.1 (LI-COR
198 Environment, USA) as half-hourly averages. The data quality flagging system and advanced
199 options for EddyPro were set up following Jammet et al. (2017). The wind vector was rotated by
200 a double rotation method and data were averaged by block averaging (Aubinet et al. 2012). The
201 time lag was obtained by maximizing the covariance (Aubinet et al. 2012).

202 Based on the wind direction, the half-hourly data were divided into western and eastern datasets,
203 similarly to analyses by Jackowicz-Korczyński et al. (2010) and Jammet et al. (2015, 2017). The
204 eastern dataset contained fluxes and other variables recorded when the wind was from 45°-135°,
205 and the western dataset parameters when wind directions were 225°-315°. These two datasets
206 were analyzed separately. Fluxes measured with wind from these two sectors are influenced by
207 mire surfaces dominated by differing permafrost status, moisture regimes, and plant community
208 structures. These reflect the thaw stages of a dynamic arctic land surface, responding to the
209 warming climate. These two wind sectors include more than 80 % of all data during the years
210 2014-2016. Northerly and Southerly wind directions, i.e. winds from outside these sectors
211 occurred mainly in low wind speed conditions. The distribution of wind directions is presented in
212 Figure 1.

213 CH₄ fluxes were filtered by quality flags according to Mauder and Foken (2004). These indicate
214 the quality of measured fluxes, “0” being the best quality fluxes, “1” being usable for annual
215 budgets, and “2” being flux values that should not be used for any analysis. Thus, in further
216 analysis fluxes with flag “2” were removed. Also, consecutive data points originating from the two
217 pre-defined wind direction sectors were removed to avoid influences from non-stationary conditions.
218 We also analyzed the behavior of the CH₄ fluxes against low turbulence conditions using friction
219 velocity (u^*) as a measure of turbulence. We binned the CH₄ fluxes into $0.05 \text{ m s}^{-1} u^*$ bins and
220 plotted the binned CH₄ flux values against u^* in 40-day windows over the growing period (d.o.y.
221 150-250, d.o.y. 210 was the beginning of the last averaging window). The CH₄ flux showed no
222 dependence on u^* below 0.6 m s^{-1} . A slight positive correlation was found during stronger
223 turbulent conditions ($u^* > 0.6 \text{ m s}^{-1}$), but we deemed this not high enough to warrant exclusion
224 of those points from further analysis. Thus, we did not remove data based on the results of u^* .
225 The fraction of data remaining, after filtering based on the quality flags and other criteria
226 described above, is presented in Table 2.

227 The analysis of relations of CH₄ fluxes to environmental parameters was done using the non-gap-
228 filled dataset of daily averages, to avoid the danger of circular reasoning of analyzing the relations
229 to the same factors that were used for gap-filling.

230

231 2.5 Footprint modeling and land cover classification

232 A detailed land cover classification was performed for the EC-tower footprint area to estimate
233 the flux contribution from the drained palsa and the thawing wet areas. We used images over
234 the Stordalen Mire collected with an eBee (SenseFly, Lausanne, Switzerland) Unmanned Aerial
235 Vehicle (UAV) carrying a Parrot Sequoia camera (Parrot Drone SAS, Paris, France) on July 31, 2018.
236 The images were processed in Agisoft Photoscan (Agisoft LLC, St. Petersburg, Russia) to create an
237 orthomosaic and a Digital Surface Model (DSM) with spatial resolutions of $50 \text{ cm} \times 50 \text{ cm}$. Field
238 data for training a classification were collected in mid-August 2018 with sampling areas of 50 cm
239 $\times 50 \text{ cm}$ that were classified into wet or dry, and a random forest classification was performed to
240 classify the footprint into wet and dry areas with the orthomosaic and DSM as input. The dry
241 areas in the flux footprint areas of SE-Sto footprint correspond to palsas, while the wet areas are
242 thawing surfaces.

243 Flux footprints were calculated with the FFP model (Kljun et al. 2015). Receptor height, Obukhov
244 length, standard deviation of lateral velocity fluctuations, friction velocity, and roughness length
245 were used as input data. The input data were divided into the two wind sectors mentioned above,
246 before footprint calculation, and footprints were calculated separately for them. We calculated
247 footprints for each half-hourly data point and aggregated these to annual footprint climatologies
248 for each sector separately. I.e. the half-hourly footprint function values were aggregated for each
249 land cover grid cell ($50 \text{ cm} \times 50 \text{ cm}$) to derive a footprint-weighted flux contribution per pixel.

250 Based on the land cover classification and annual CH₄ fluxes for each sector, combined and
251 weighted with the footprint climatology, it was possible to estimate annual emissions from the
252 different surface type.

253

254 2.6 Gap-filling methods for CH₄

255 We compared four different gap-filling methods, separately for both sectors. These methods
256 were: look-up tables (REddyProc (“Jena gap-filling tool”), Wutzler et al. 2018), 5-day moving
257 mean, artificial neural network (Jammet et al. 2015, 2017), and generalized linear models (Rinne
258 et al. 2018). All these methods, except for moving mean, have been used before for gap-filling
259 CH₄ flux data from different mire ecosystems. The look-up table approach uses half-hourly data,
260 while for the other three methods we used daily average data, as CH₄ emissions from this
261 ecosystem do not show a diel cycle (see below, Section 3.2 for a detailed description).

262 The uncertainties due to each method were analyzed by the introduction of artificial gaps to the
263 data, with lengths comparable to gaps existing in the year 2014. 35-day and 80-day gaps were
264 implemented to the data of years 2015 and 2016. Gaps were placed in the winter period, to
265 obtain similar gap distribution as in the year 2014 (gap distribution is presented below in Table
266 3). Annual sums, with artificial gaps, were compared with results from methods without those
267 gaps. Statistical significances of differences between models were analyzed by using a two-
268 sample t-Test for equal means with a 95 % confidence level (MATLAB R2019b).

269

270 2.6.1 REddyProc

271 The Jena gap-filling tool using look-up tables requires half-hourly data of CH₄ flux and
272 environmental data: shortwave incoming radiation, air temperature, soil temperature, relative
273 humidity, and friction velocity. Based on environmental data, fluxes are classified and averaged
274 within a given time window. The missing data are then filled with the average value from
275 classified data. Uncertainty can be estimated as standard deviations of fluxes within classes.
276 Detailed information about the method is presented by Falge et al. (2001) and Wutzler et al.
277 (2018).

278

279 2.6.2 Moving average

280 A 5-day moving mean approach is a very simple gap-filling method where the moving mean is
281 calculated for subsets of the data. In case of a gap in the averaging window, the mean value is
282 calculated for fewer observations. The method was applied on daily average CH₄ flux data using
283 MATLAB (movmean function). For gaps longer than 5 days, linear interpolation was used
284 between the last point before the gap and the first point after gap. Uncertainties of the single
285 gap-filled flux were estimated by calculating the moving standard deviation (movstd function,
286 MATLAB) on the same subset of the data like for the moving mean.

287

288 2.6.3 Artificial Neural Network

289 An artificial neural network (ANN) has been successfully applied for gap-filling of CH₄ fluxes by
290 e.g. Dengel et al. (2013), Jammot et al. (2015,2017), Knox et al. (2016) and Rößger et al. (2019).
291 This type of ANN was designed in MATLAB using a fitnet function with 30 hidden neurons. We
292 used the Levenberg-Marquardt algorithm as a training function (Levenberg 1944 Marquardt
293 1963). All available daily average CH₄ values were used to train (70 %), validate (15 %), or test (15
294 %) the ANN. The ANN requires input data without gaps to work properly and thus the short gaps
295 (up to three days) in environmental daily averaged data were filled by linear interpolation before
296 the ANN analysis. All environmental variables, except the WTL were used as input for the ANN
297 method. The WTL was excluded because it was not available during the frozen period, i.e. most
298 of the year. The ANN method was applied to sectors and each year separately (ANN YbY) or all
299 three years together. Multiple repetitions were done to minimize uncertainty connected with
300 randomly chosen data points for training, validation, and testing. The network was trained and
301 used to calculate the time series of CH₄ daily fluxes 100 times in each case of gap-filling. The
302 number of repetitions was chosen to have a sample large enough to calculate reliable mean and
303 standard deviation values, and to keep the computation time reasonably short. An average CH₄
304 flux for each day was calculated based on 100 daily values. The gaps in the measured flux time
305 series were filled with values from the time series calculated by ANN. Errors were estimated as
306 standard errors of mean on daily flux, based on 100 ANN trained values.

307

308 2.6.4 Generalized Linear Model

309 Generalized linear models (GLM) are linear combinations of linear and quadratic functions
310 describing the dependence of response variables to predictors. In our case, the response variable
311 was the logarithm of daily average CH₄ flux, and predictors were daily averages of measured
312 environmental variables. Controlling factors of CH₄ emission were examined by a procedure
313 similar to the routine described by Rinne et al. (2018). A correlation matrix of linear correlation
314 based on daily values of environmental factors and CH₄ fluxes was constructed (Figure S3).
315 Additionally, the logarithm of CH₄ fluxes was added to the correlation matrix to check the
316 exponential relationship between parameters. This type of relationship between CH₄ fluxes and
317 peat temperature was previously found by e.g. Christensen et al. (2003), Jackowicz-Korczyński et
318 al. (2010), Bansal et al. (2016), Pugh et al. (2017) and Rinne et al. (2018). Gap-filled CO₂ flux, and
319 gross primary production (GPP), were also included as prospective controlling factors. In order to
320 avoid strong cross-correlation between predictors, first, we selected the parameter with the
321 highest correlation and then removed parameters from the GLM development with a cross-
322 correlation between parameters $R^2 > 0.6$. We thus chose GPP, soil temperature at 30 cm depth
323 for the eastern sector and 10 cm depth for the western sector, soil water content (SWC), short-
324 wave incoming radiation, and vapor pressure deficit (VPD) as possible predictors. The model was
325 constructed in MATLAB using the stepwiseglm function (Dobson 2002). The GLM was made

326 separately for each year (GLM YbY) and for all three years combined. Errors were estimated as
327 95 % confidence intervals because it was an output of the stepwise function. This method was
328 also used for the determination of the controlling factors from the possible predictors.

329

330 2.7 Gap-filling of CO₂ fluxes

331 CO₂ fluxes were calculated for both wind sectors. CO₂ flux exhibited a diel pattern in the growing
332 season, with uptake during daytime (shortwave incoming radiation > 50 W m⁻²) and release at
333 night (shortwave incoming radiation < 50 W m⁻²). We used the ANN to gap-fill the time series of
334 CO₂ fluxes. This method was chosen to check the possibility to reconstruct the diel cycle. This diel
335 pattern of CO₂ was taken into account by using half-hourly data. We used all environmental
336 variables excluding the WTL, as for CH₄ fluxes. GPP was obtained by partitioning the gap-filled
337 data using the Jena gap-filling tool. Finally, the half-hourly gap-filled GPP and CO₂ data were
338 averaged to daily values.

339

340 2.8 Contribution of palsa and thaw surfaces to average CH₄ emission

341 Using the average annual CH₄ emission from the two wind sectors and the relative contributions
342 of the two surface types to the fluxes from these sectors, we calculated the average annual
343 emission from these surface types. We expressed the average annual CH₄ fluxes for the two
344 sectors, F_e (East) and F_w (West), with a pair of equations,

$$345 F_e = f_{e,p}E_p + f_{e,t}E_t, \quad (1)$$

$$346 F_w = f_{w,p}E_p + f_{w,t}E_t, \quad (2)$$

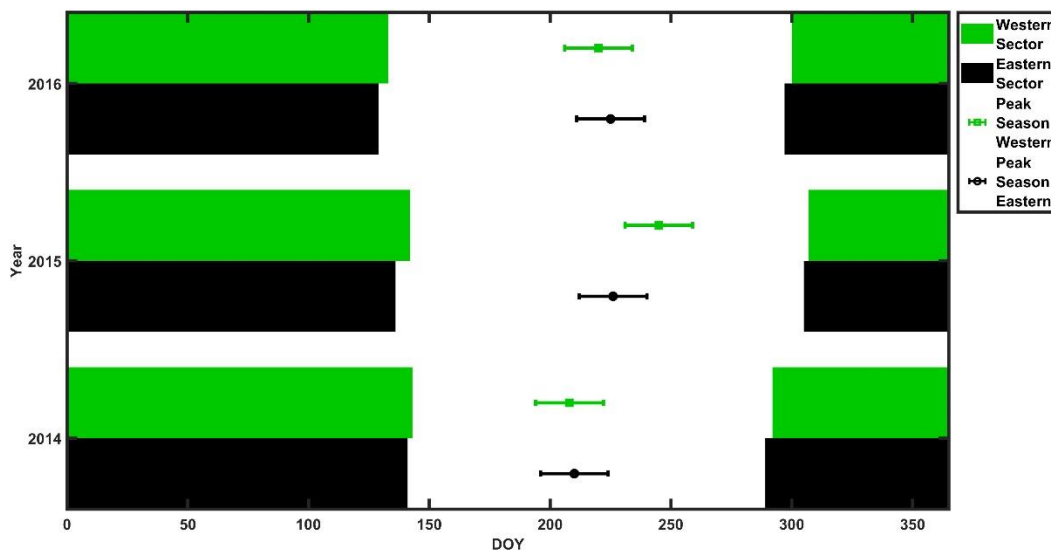
347 where f indicates the fractional contribution of surface type to the flux from the footprint
348 calculations (subscripts e and w referring to east and west, respectively; p and t to palsa and thaw
349 surface, respectively); and E_p and E_t are emissions from palsa and thaw surface, respectively. We
350 solved this equation set with two unknowns to yield E_p and E_t . Here we assumed that the emission
351 rate from both palsa and thaw surfaces are equal in eastern and western sectors. Furthermore,
352 we must assume that there is no correlation between footprint contribution and seasonally
353 developing emission rate at either surface type. The seasonally constant contributions of the
354 surface types to the footprint indicate that the latter assumption may well be valid (Figure S4).

355 2.9 Definition of seasons

356 The beginning of the unfrozen period was defined as the day when daily averages of peat
357 temperature at 10 cm depth had been above 0 °C for three consecutive days. The end of the
358 unfrozen period was defined as the day when daily averages of peat temperature at 10 cm depth
359 had been below 0 °C for three consecutive days. The unfrozen and frozen periods commence in
360 the western sector on average 3 days earlier than in the eastern sector, but differences in the
361 unfrozen season length are not systematic (Figure 2). The beginning and the end of the unfrozen

362 season were determined independently for both sectors. The horizontal distance between soil
 363 temperature sensors in eastern and western sectors was around 75 m, differed about 2 m in
 364 elevation, and the distance from the flux tower was roughly 40 m.

365



366

367 Figure 2. Time periods of frozen peat during the years 2014 - 2016 (green and black bars) and
 368 peak CH₄ emission season (dot with whiskers) for the western sector (green) and the eastern
 369 sector (black). (For peak season definition see Section 3.2)

370

371 3 Results

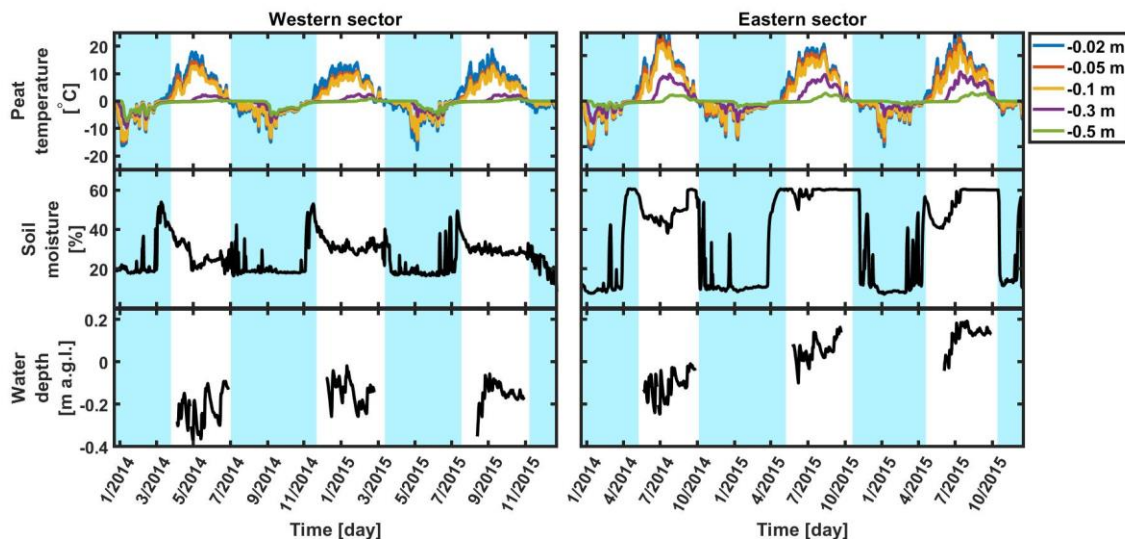
372 3.1 Environmental conditions and flux footprints

373 Winds from eastern and western sectors contributed to 50 % and 40 % to the daytime wind
 374 directions, respectively (Figure 1). Northerly and southerly winds contributed to around 5 % each.
 375 In the nighttime, 51 % of wind was from the East and 32 % from the West. Additionally, 15 % of
 376 total wind came from the South during nighttime, probably as catabatic flow from higher
 377 mountain areas. The wind from North was rare, around 2 % of all the cases.

378 The annual average peat temperature of the uppermost 50 cm of peat was systematically warmer
 379 in the eastern sector than in the western sector (Table 1; Figure 3). However, the summertime
 380 peat temperature at the top 10 cm layer was warmer for the western sector (Figure S5). The
 381 situation was the opposite during winter when the western sector down to 50 cm was colder
 382 than the eastern sector. During our investigation period (2014-2016), the peat temperatures
 383 from 30 cm to 50 cm below ground were colder in the western sector than those of the eastern
 384 sector, corresponding to the existence of the permafrost. Temperature differences, between
 385 both areas, at the same depth, were stable over the measurement years. The biggest difference

386 was noticed at a depth of 30 cm. The temperatures at 30 cm and 50 cm depth were increasing
 387 during consecutive years.

388



389
 390

391 Figure 3. Time series of daily mean values for western and eastern sectors for: peat temperature (top
 392 panel), soil moisture (middle panel), and water table level (bottom panel), where the shaded light blue
 393 area is the frozen period, when peat temperature at 10 cm was below 0 °C (see Section 2.8 for a detailed
 394 description).

395

396 Table 1. Mean annual air and peat temperatures for the years 2014-2016 for eastern and western
 397 sectors.

depth in cm	Temperature [°C]								
	2014 E	2014 W	2014 E-W difference	2015 E	2015 W	2015 E-W difference	2016 E	2016 W	2016 E-W difference
ambient air	0.3	0.3	-	0.1	0.1	-	0.3	0.3	-
2	1.6	1.4	0.2	2.2	2.0	0.2	2.2	1.9	0.2
5	1.4	0.8	0.5	1.9	1.3	0.7	1.9	1.3	0.6
10	1.2	0.5	0.6	1.7	1.1	0.7	1.7	1.1	0.6
30	0.3	-0.9	1.2	0.6	-0.6	1.2	0.8	-0.5	1.3
50	-0.1	-1.0	0.8	0.0	-0.8	0.8	0.2	-0.6	0.8

398

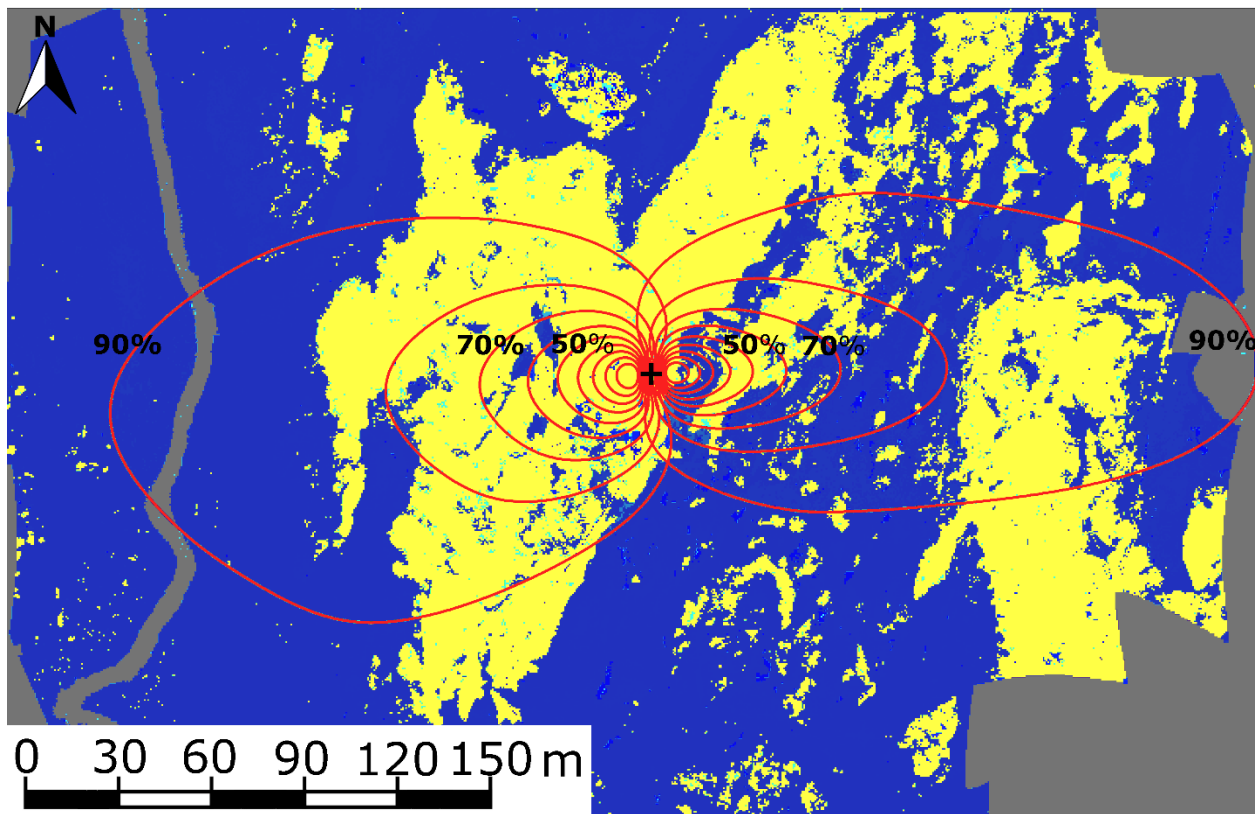
399 The WTL was higher in 2014 than in 2015 and 2016 according to measurements both in the
 400 eastern and western sectors (Figure 3). This is not reflected in the SWC measurements, which is
 401 probably due to the different locations of the measurements of WTL and SWC. In the western
 402 sector the WTL was measured in an isolated wet patch, surrounded by drier palsa and thus it is

403 not representative of the dominating type of this area. The WTL in the eastern sector was more
404 representative of the area of the footprint. Data from the WTL probe in the West part of the mire
405 was excluded from the further analysis as it does not represent the situation for the majority of
406 the western sector. The soil moisture was higher for the eastern than the western sector during
407 all years. The data shows a distinctive step change at thaw and freeze, as the dielectricity of ice
408 and liquid water differ. In the eastern sector, the soil was fully saturated for most of the unfrozen
409 period during the years 2015-2016, while 2014 indicates lower water content levels. The western
410 sector was never fully saturated at any time during the years 2014-2016.

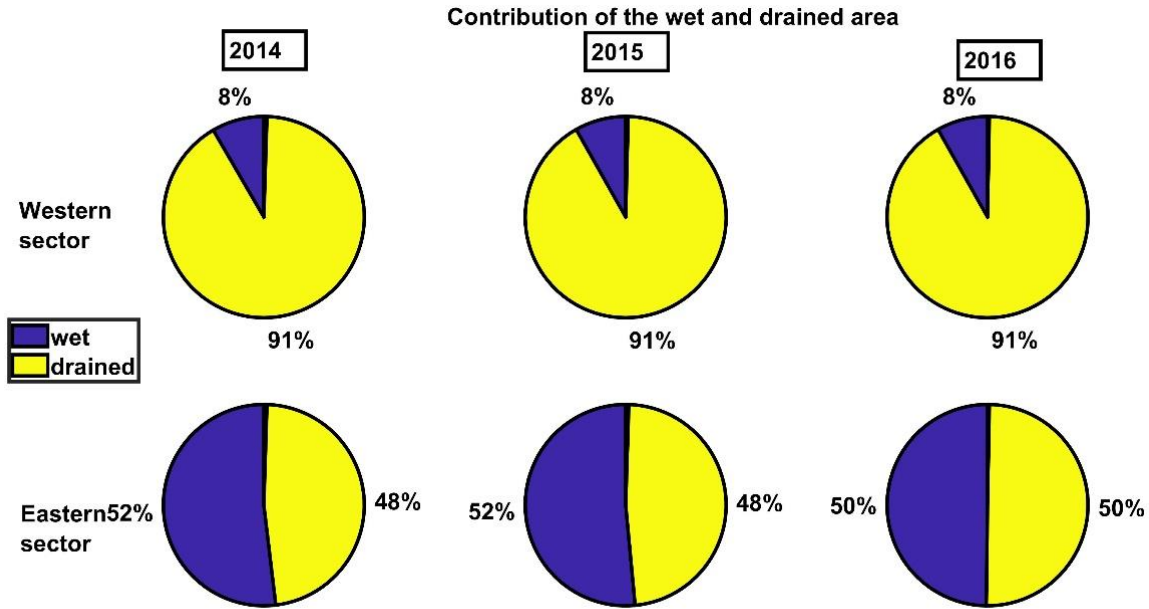
411 Footprint and flux contribution of drier and wetter areas are presented in Figure 3. The dry areas
412 (yellow) contribute on average over all three years to more than 90% of the fluxes measured
413 from the western sector at the eddy covariance tower. In the eastern sector, the wetter (blue)
414 and drier areas contribute almost equally to the fluxes. The contributions of the wet and dry
415 areas to the fluxes in both sectors remained almost constant across the three study years.

416

417



418



419

420 Figure 4. Footprint-weighted contribution of the wet and drained area at the SE-Sto tower (upper panel)
 421 for the year 2014 and relative amounts of wetter areas (blue) and drained palasa area (yellow) inside the
 422 80 % area of influence of the footprints (lower panel). The black cross is the location of the tower and
 423 each red line indicates 10 % of the contribution from the source area to measured fluxes at the tower.
 424 The footprint climatology is almost identical for all study years, see bottom panel.

425

426 3.2 CH₄ fluxes

427 We analyzed the growing season data of each year and both wind sectors separately in regards
 428 to a possible diel cycle of CH₄ fluxes. This was done by normalizing each half-hourly flux by
 429 dividing it with the daily median from that day for the whole growing season (Rinne et al. 2007).
 430 This yielded a normalized diel cycle of CH₄ fluxes. Figure S6 shows slightly lower emission during
 431 mid-day hours. However, the difference is small compared to the short term variation in the
 432 fluxes as indicated by the interquartile range. Thus, for the purpose of gap-filling this effect could
 433 be negligible in calculating daily averages. However, it is interesting to observe this type of diel
 434 cycle, with minima at daytime. It could be linked to the temperature cycle of the top peat layer.
 435 This could affect the methanotrophy, while the methanogenesis occurring at slightly deeper
 436 layers would be less affected. This would lead to higher methanotrophy at daytime and thus
 437 lower emission. It is possible to calculate CH₄ daily averages without gap-filling the diel cycle,
 438 similarly to e.g. Rinne et al., (2007, 2018) and Jackowicz-Korczyński et al. (2010). We discarded
 439 daily averages with less than 10 flux data points from further analysis, to ensure the reliability of
 440 the daily average fluxes. Uncertainties of daily averages were calculated as standard errors of the
 441 mean. The size of the available flux dataset, after gap-filling by daily averaging, is presented in
 442 Table 2. The gap distribution in the datasets for the different sectors and years is presented in
 443 Table 3.

444

445 Table 2. The size of available daily data sets after gap-filling by daily averaging for each year and
 446 wind sector.

	2014 E	2015 E	2016 E	2014 W	2015 W	2016 W
total number of points	365	365	366	365	365	366
number of points after averaging	137	174	182	96	167	178
% of available data	38	48	50	26	46	49
% of available data during winter period	36	54	56	12	36	37
% of available data during unfrozen period	40	41	42	47	58	63

447

448 Table 3. Gaps distribution over years and wind direction.

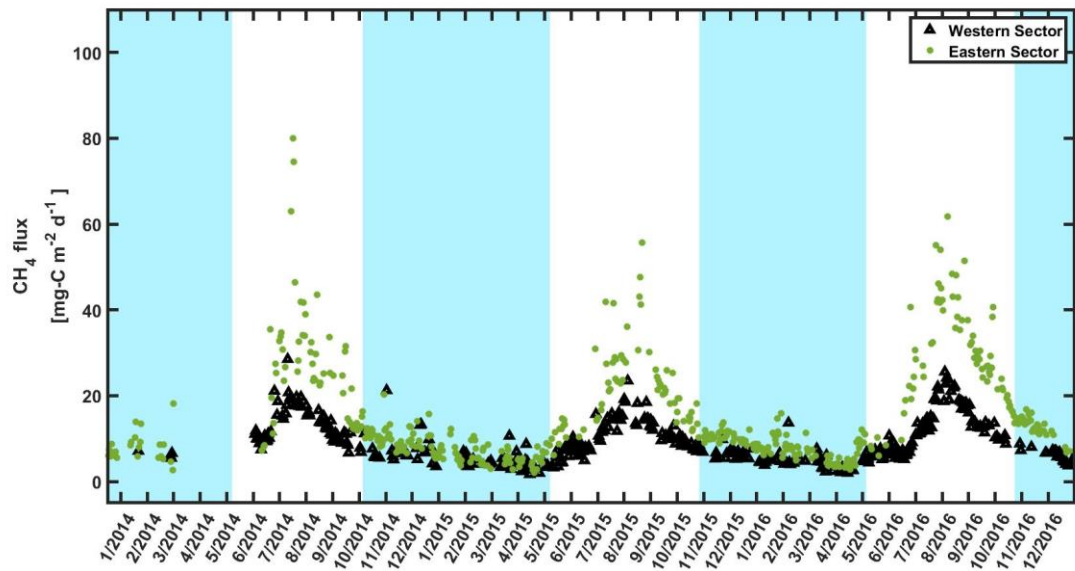
Type of gap	Length of gap	2014 E	2015 E	2016 E	2014 W	2015 W	2016 W
short gap	1-3 day	32	50	41	24	44	36
medium gap	4-7 day	7	12	11	6	8	11
long gap	8-30 day	3	7	4	4	6	6
very long gap	> 30 day	1	0	0	3	0	0

449

450 Daily non-gap-filled CH₄ fluxes showed a characteristic annual cycle, with peak emissions in
 451 August (Figure 5) and low but positive wintertime fluxes. Wilcoxon rank sum test need data
 452 without autocorrelation. The autocorrelation in the data existed up to 8 days. Based on this we
 453 divided winter data with subsets where every 9th day was selected. We tested the difference of
 454 those subsets to zero with Wilcoxon rank sum test. Winter fluxes were statistically different from
 455 zero ($p < 0.001$, two-sided Wilcoxon rank sum test). Winter fluxes from the western and eastern
 456 sectors were also different from each other ($p < 0.001$).

457 CH₄ fluxes, both from the western sector and the eastern sector started increasing after
 458 snowmelt up to a maximum in August (Figure 5). No major springtime emission burst nor autumn
 459 freeze-in burst were observed in any of the years.

460



461
 462 Figure 5. Time series for non-gap-filled CH₄ daily averaged fluxes for the western sector (green triangles)
 463 and the eastern sector (black dots), where the shaded light blue area is frozen period when peat
 464 temperature at 10 cm was below 0 °C (see Section 2.8 for a detailed description).

465
 466 The middle-day of the peak season of the CH₄ emission was defined as the maximum of the 14-
 467 days moving average. Two weeks forward and backward from the middle-day was defined as the
 468 peaks season and emissions were estimated for that period in each year. The average emission
 469 during the peak seasons was 40 mg-C m⁻² d⁻¹ for the eastern sector and 19 mg-C m⁻² d⁻¹ for the
 470 western sector. Detailed emissions for all years are presented in Table 4. The peak season
 471 emissions were statistically different from each other (p < 0.001). Wintertime fluxes were steadily
 472 declining as winter continued and the lowest emissions were observed slightly before the spring
 473 thaw. Wintertime average emissions were 9 mg-C m⁻² d⁻¹ for the eastern sector and 6 mg-C m⁻²
 474 d⁻¹ for the western sector. Detailed emissions of winter periods are presented in Table 5.

475 Table 4. CH₄ emission during the peak season

	Mean	Standard deviation	The standard error of the mean
	[mg-C m ⁻² d ⁻¹]		
2014 E	40.7	17.2	4.3
2015 E	34.4	11.7	3.7
2016 E	45.4	6.7	1.7
2014 W	18.6	3.2	0.8
2015 W	16.1	3.2	1.0
2016 W	20.9	2.6	0.7

477 Table 5. CH₄ emission during the winter period

	Mean	Standard deviation	The standard error of the mean
	[mg-C m ⁻² d ⁻¹]		
2014 E	9.0	2.8	0.4
2015 E	8.3	1.7	0.2
2016 E	9.8	2.6	0.3
2014 W	7.2	2.2	0.4
2015 W	5.5	1.4	0.2
2016 W	5.2	3.4	0.4

478

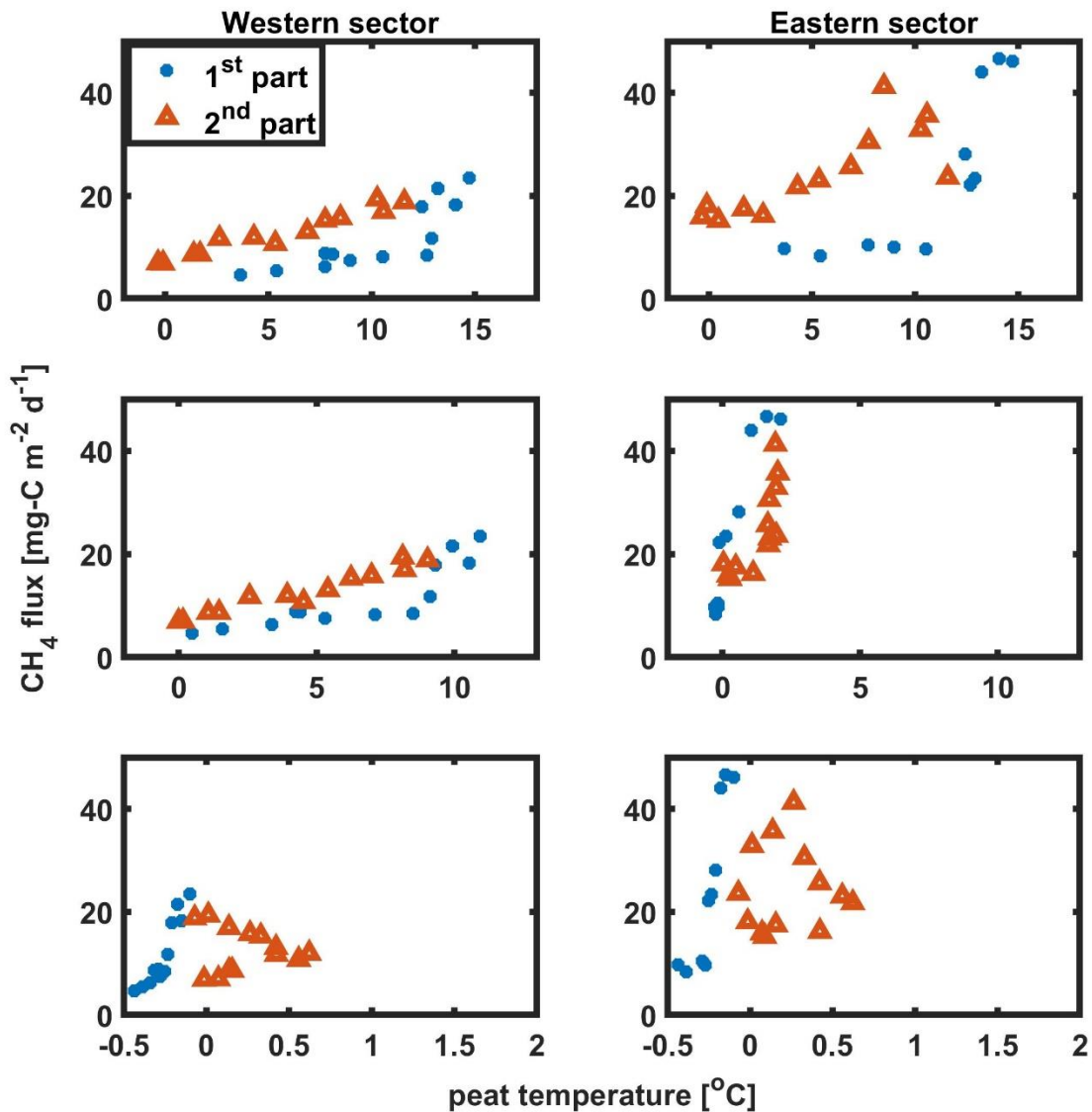
479

480

3.3 Factors controlling the CH₄ fluxes

481 In the eastern sector, the CH₄ flux correlated best with the peat temperature at 30 cm depth, and
 482 in the western sector with the temperature at 10 cm depth. Using temperatures above the level
 483 of maximum correlation led to similar hysteresis-like behavior in CH₄ flux - temperature relations
 484 as presented by Chang et al. (2020), but using deeper temperatures led to inverse hysteresis
 485 compared to shallower temperatures (Figure 6). The correlation matrix (Figure S3) shows the
 486 importance of SWC in the CH₄ emissions, while WTL does not correlate significantly with CH₄ flux.
 487 Controlling factors were examined before and after temperature normalization of the CH₄ fluxes
 488 following Rinne et al. (2018) (Table 6), in order to avoid effect of cross-correlation between
 489 explanatory parameters.

490



491

492 Figure 6. Weekly averages of CH₄ fluxes against the surface peat temperature (top panels), the depth
 493 with best correlation (middle panels), and the deeper layer (bottom panel). Data were divided into the 1st
 494 part of the growing season (blue dots) before the maximum weekly emission, and 2nd part of the growing
 495 season (orange triangles) after that.

496 The result from GLM, showing the variables that contribute to the model, is presented in Table
 497 S2. The parameter that was selected first by all models, was peat temperature, at 10 cm depth
 498 for the western sector and at 30 cm depth for the eastern sector. For the eastern sector, the GLM
 499 algorithm selected SWC as the explanatory factor for CH₄ fluxes during all years as well as for the
 500 combined three-year period. The GLMs created for the western sector did not have other
 501 explanatory factors besides the peat temperature that were selected in all years. However, two

502 more explanatory factors, GPP and shortwave incoming radiation, appeared in the three time
 503 periods (years 2015 and 2016, and three-years combined) for the western sector.

504 The eastern sector models had shortwave incoming radiation as the explanatory factor for the
 505 year 2015, the year 2016, and combined three-year period. A unique variable for this sector was
 506 the vapor pressure deficit, which was used in the models constructed for the years 2016 and
 507 combined three-year period.

508 The year 2014 was characterized by a smaller number of parameters contributing to the models
 509 for both sectors compared to other years and combined three-year models. Only peat
 510 temperature and SWC were explanatory variables for both sectors in this year. The years 2015
 511 and 2016 and all three years combined have a longer list of parameters.

512 As the WTL data was available only during a short period of the year, it was not analyzed with the
 513 GLM. The WTL measurement in the western sector was not representative of the conditions for
 514 most of the sector, this parameter was not used for further analysis from this sector. The WTL
 515 was correlated with CH₄ fluxes for the eastern sector.

516 Based on the chosen explanatory variables it was noticed that the seasonal cycle could be
 517 explained by a lower number of parameters than the interannual variation.

518 Table 6. Summary of controlling factors before and after temperature normalization

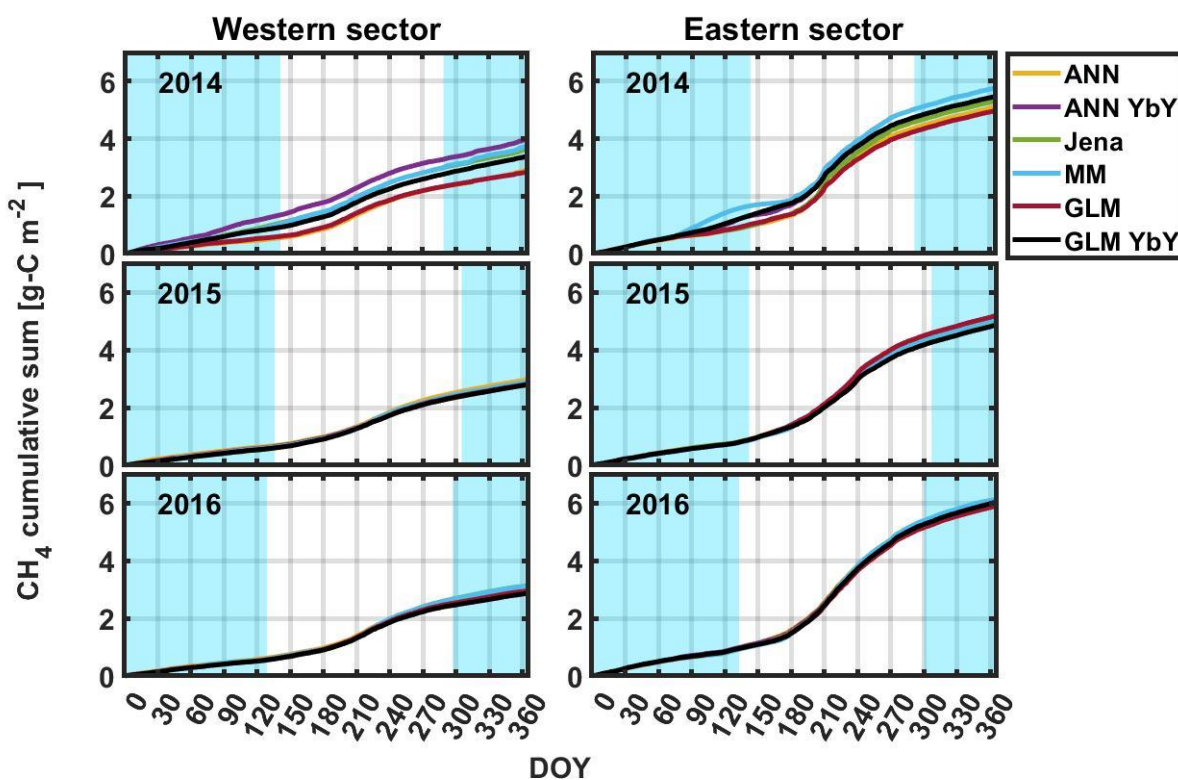
Year and ecosystem	R for CH ₄ flux	the p-value for CH ₄ flux	R for temperature normalized CH ₄ flux	the p-value for temperature normalized CH ₄ flux
GPP				
2014 E	0.71	7x10 ⁻²²	-0.03	0.70
2015 E	0.69	2x10 ⁻²⁵	0.02	0.83
2016 E	0.77	1x10 ⁻³⁶	0.21	4x10 ⁻³
2014 W	0.69	4x10 ⁻¹⁵	-0.10	0.36
2015 W	0.73	6x10 ⁻²⁹	0.05	0.56
2016 W	0.71	5x10 ⁻²⁹	-0.02	0.76
WTL				
2014 E	-0.50	2x10 ⁻⁴	1x10 ⁻²	0.94
2015 E	-0.20	0.30	-0.20	0.17
2016 E	0.60	4x10 ⁻⁶	-0.30	0.01
SWC				
2014 E	0.51	2x10 ⁻¹⁰	-0.02	0.79
2015 E	0.51	1x10 ⁻¹²	-0.03	0.66
2016 E	0.69	1x10 ⁻²⁶	0.20	6x10 ⁻³
2014 W	-0.31	2x10 ⁻³	-0.37	2x10 ⁻⁴
2015 W	0.19	0.02	-0.19	0.02
2016 W	0.22	3x10 ⁻³	-0.26	5x10 ⁻⁴

519

520

521 3.4 Gap-filled annual cycles

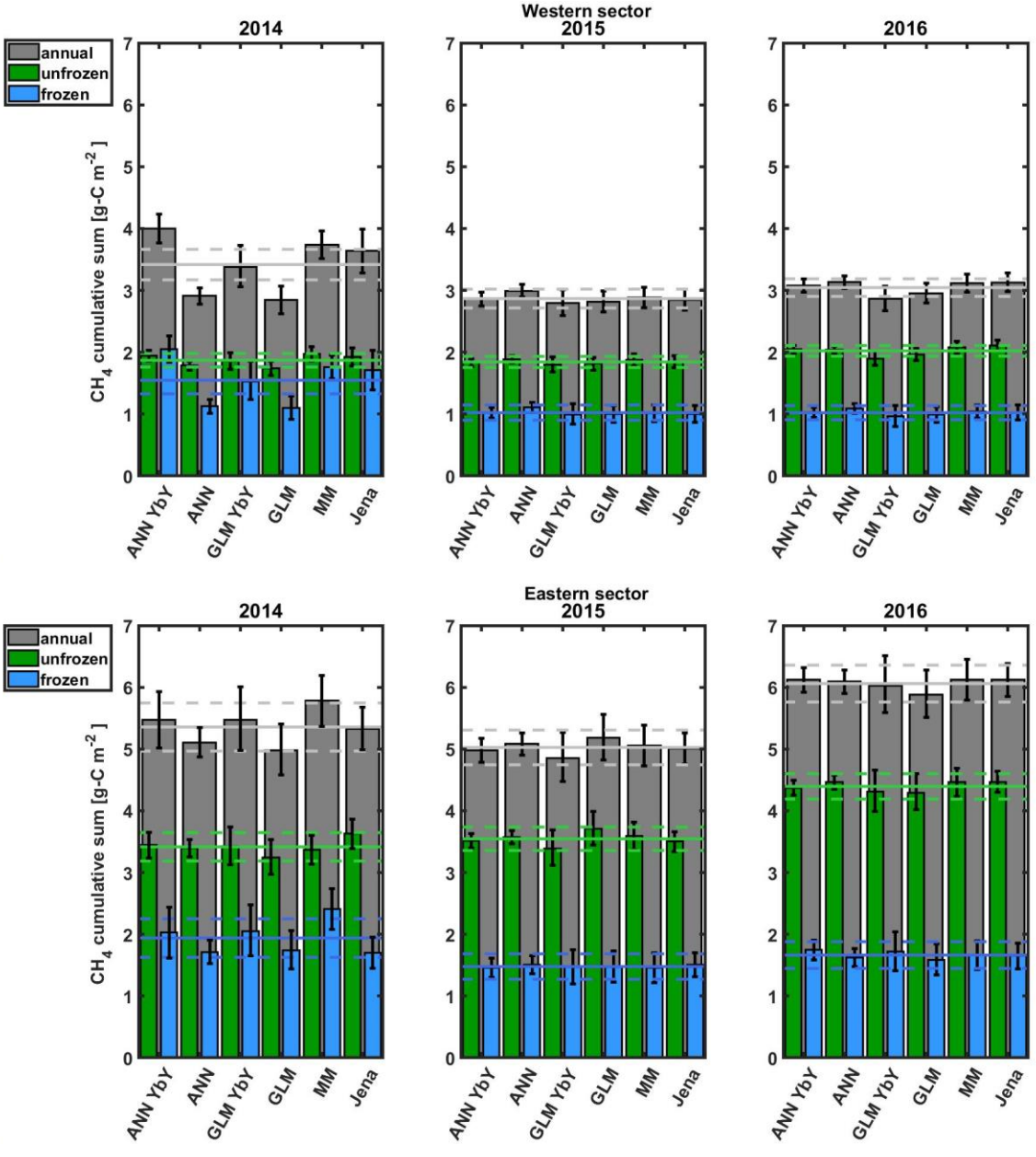
522 Cumulative CH₄ emissions based on different gap-filling methods are presented in Figure 7. All
523 follow a similar annual curve, with a steeper increase in summer, but also relatively high
524 wintertime contribution. Annual, wintertime, and unfrozen period emissions by all gap-filling
525 methods, with their estimated uncertainties, are shown in Figure 8. Emission estimation by each
526 sector and data gap-filled by the different method are presented in Table S3. Average values from
527 all models with their upper and lower limit and wintertime contribution to fluxes are
528 demonstrated in Table 7.



529

530 Figure 7. The cumulative sum of CH₄ fluxes for the years 2014-2016 for western and eastern sectors
531 calculated with the different gap-filling methods. ANN - the artificial neural network for all years, ANN
532 YbY - artificial neural network each year separately, Jena - Jena online gap-filling tool, MM - moving
533 mean with 5-day moving window, GLM- the general linear model for all years, GLM YbY - the general
534 linear model for each year separately. The shaded light blue area designates the frozen period when
535 peat temperature at 10 cm was below 0 °C (see Section 2.8 for a detailed description).

536



537

538

539 Figure 8. Comparison of cumulative sums of CH₄ fluxes for different gap-filling methods for the western
 540 sector (top panel) and eastern sector (bottom panel). ANN - the artificial neural network for all years, ANN
 541 YbY - artificial neural network each year separately, Jena - Jena online gap-filling tool, MM - moving mean
 542 with 5-day moving window, GLM- the general linear model for all years, GLM YbY - the general linear
 543 model for each year separately. Gray bars are for the annual sums, blue bars are for the frozen period
 544 sums and green bars are for the unfrozen period (see Section 2.8 for a detailed description). Solid lines
 545 are the mean value from all models and dashed lines are for the standard deviation range, with the same
 546 colors described above.

547

548

549 As can be seen in Table 3, the year 2014, with a larger difference between annual emissions
 550 calculated by different gap-filling methods, had very long gaps that were not present in other
 551 years. Also, the uncertainties in annual emission are the largest for the year 2014 for all gap-filling
 552 methods, reflecting the gap distribution.

553

554 Table 7. Average CH₄ annual emission based on all models with the upper and lower limit and
 555 contribution from the winter fluxes.

	Mean	Lower limit	Upper limit	Contribution to wintertime fluxes		Mean	Lower limit	Upper limit	Contribution to wintertime fluxes	
				Western sector					Eastern sector	
				g-C m ⁻² a ⁻¹					%	
2014	3.4	2.8	4.0	45		5.4	5.0	5.8	36	
2015	2.8	2.8	3.0	36		5.0	4.9	5.2	29	
2016	3.1	2.8	3.1	34		6.1	5.9	6.1	27	

556

557 Three years' averages of GPP and net ecosystem exchange (NEE) for two sectors are presented
 558 in table 8. As comparison, data from lake and tall sedge fen areas at the Stodalen mire complex,
 559 where permafrost was completely thawed, are also presented (Jammet et al., 2017). The fen has
 560 the highest percentage of carbon emitted as CH₄, as compared to the annual CO₂ uptake. The
 561 eastern and the western sectors emitted less of the assimilated carbon as CH₄ compared to the
 562 completely thawed area. The uptake of carbon as CO₂ was also largest at the fen.

563 Table 8. Average annual GPP, NEE and CH₄ emission from western and eastern sector in
 564 comparison to fen.

	GPP	NEE	CH ₄	CH ₄ /GPP	CH ₄ /NEE
	g-C m ⁻² a ⁻¹	g-C m ⁻² a ⁻¹	g-C m ⁻² a ⁻¹	%	%
Western sector	225	-28.9	3.1	1.4	19.6
Eastern Sector	257	-42.0	5.5	2.2	14.0
Fen (Jammet et al. 2017)	N.A.	-66.3	21.2	N.A.	32.0

565

566 The 3 years' annual average CH₄ emissions of palsa and thawing surfaces, as calculated by Eq. (1)
 567 and (2), are presented in Table 9. For comparison average annual emissions from other major
 568 surface types, measured by EC technique, are shown as well. The emission from the tall

569 graminoid fen, a third mire type common at Stordalen Mire, has been previously measured using
 570 the EC method by Jackowicz-Korczyński et al. (2010) and Jammet et al. (2017). In addition to
 571 these, the mire complex includes shallow lakes. Their annual CH₄ emission has been measured
 572 by EC method by Jammet et al., (2017).

573 Table 9. Annual CH₄ emission from different components of the Stordalen Mire complex from EC
 574 studies.

type of wetland	Annual emission [g-C m ⁻² a ⁻¹]	References
palsa plateau surface	2.7 ± 0.5	this study
thawing wet surface	8.2 ± 1.5	this study
thawed fen	15.8 ± 1.6	Jackowicz-Korczyński et al. 2010
thawed fen	21.2 ± 1.3	Jammet et al. 2017
shallow lake	4.9 ± 0.6	Jammet et al. 2017

575

576 4 Discussion

577 4.1 Differences in controlling factors

578 According to the GLM, peat temperature and GPP were typically the first parameters selected by
 579 the algorithm to explain CH₄ fluxes. In the eastern sector, the CH₄ flux correlated best with the
 580 peat temperature at 30 cm depth, and in the western sector with the peat temperature at 10 cm
 581 depth. Temperature as a controlling factor of CH₄ emission has been reported in many wetlands
 582 studies (Christensen et al. 2003, Jackowicz-Korczyński et al. 2010, Bansal et al. 2016, Pugh et al.
 583 2017, Rinne et al. 2007; 2018), in line with our findings. The correlation of CH₄ fluxes with the
 584 temperature at 5 cm depth was also higher than for 30 cm in the western sector. As the peat in
 585 the palsa is frozen at 30 cm depth for most of the growing season, the correlation between CH₄
 586 fluxes and temperature at these depths is lower. Temperature correlation for the upper part,
 587 2 cm, and 5 cm depth, shows a similar level of correlation as presented by Jackowicz-Korczyński
 588 et al. (2010). As they did not analyze correlation with the temperature at deeper peat, we cannot
 589 compare these results. The hysteresis-like behavior of the CH₄ flux – temperature relation is
 590 similar to that observed by Chang et al. (2020) when using temperatures measured above the
 591 depth of maximum correlation, but inversed when using temperatures measured at deeper
 592 depths (Figure 6). This is in line with at least part of the hysteresis-like behavior to be due to the
 593 lag of seasonal temperature wave at the depth of CH₄ production compared to the timing of the
 594 temperature wave at shallower depth or air temperature.

595 GPP was indicated as a controlling factor for CH₄ emission from a boreal fen ecosystem by Rinne
 596 et al. (2018). In our study, the correlation matrix shows a significant correlation between daily
 597 average GPP and CH₄ flux at both sectors (Table S3). To disentangle the confounding effects of
 598 temperature and GPP, we used temperature-normalized CH₄ fluxes following Rinne et al. (2018)
 599 which revealed that the correlation between GPP and temperature-normalized CH₄ flux was not
 600 significant in most years (Table 6). Only the data from the eastern sector in the year 2016 shows
 601 a significant correlation. Thus, it seems hard to disentangle the effects of temperature and GPP

602 on CH₄ fluxes using this data set. As our data set consists of only three years, the analysis of
603 interannual variations would not be a robust approach either.

604 Solar shortwave incoming radiation was selected as a controlling variable by 6 of 8 GLM models
605 (Table S3). This parameter has an indirect effect on CH₄ production via photosynthesis and
606 subsequent substrate production. The maximum emission of CH₄ occurs later in the year than
607 maximum radiation. This may be due to the CH₄ emission depending on the deeper peat
608 temperature or seasonal cycle of available substrates, lagging behind the annual cycle of
609 radiation (e.g. Rinne et al., 2018; Chang et al., 2020). The negative contribution of shortwave
610 radiation in GLM can be due to the slight diel cycle of CH₄ emission, with lowest values at
611 daytime. Mechanistically we can think that the solar irradiance will heat the top of the peat layer,
612 thus leading to increased methanotrophy at daytime (see discussion above on diel cycle). This
613 can lead to situation where the methanotrophy is higher in sunny days with warm surface and
614 lower in cloudy days. The role of photosynthesis for the substrate supply of methanogenesis is
615 likely to act in the seasonal time scale, where its effect can be masked by the strong correlation
616 between peat temperature and CH₄ emission. The highest correlation of CH₄ flux and radiation
617 was observed in 2014, but GLM did not select radiation as an explanatory factor for this year.
618 Other years and the whole period show a much lower correlation.

619 CH₄ fluxes from wetlands have been shown to depend on WTL in many studies (e.g. Bubier et al.,
620 2005; Turetsky et al., 2014; Rinne et al., 2020). However, in a number of studies, the CH₄ fluxes
621 have shown to be relatively insensitive to the small variation, without strong extreme conditions,
622 in the WTL (Rinne et al. 2007, 2018, Jackowicz-Korczyński et al. 2010). In the eastern sector, CH₄
623 flux and WTL were correlated for the years 2014 and 2016. However, after normalization of CH₄
624 fluxes with their temperature dependence following Rinne et al., (2007), correlations were
625 mostly not significant (Table 6). This is similar to conclusions drawn by e.g. Rinne et al. (2007,
626 2018) and Jackowicz-Korczyński et al. (2010).

627 Instead of WTL, we used SWC as a possible controlling factor for the CH₄ emission from the
628 western sector. Sturtevant et al. (2012) also reported SWC as a controlling factor in autumn. SWC
629 shows correlation on a significant level before and after normalization for three years for the
630 western sectors (Table 6).

631 The GLM algorithm selected SWC as one of the explaining factors while constructing the GLM for
632 the eastern sector for the whole measurement season. It was chosen by models built for three
633 years together and each year separately. R and p-value are presented in Table 6. A reduction of
634 R and increase in p-value after temperature normalization is similar to previous parameters. The
635 correlation of CH₄ emission with SWC stays on a significant level only in the year 2016.

636

637 [4.2 Gap-filling methods](#)

638 In general, the gap-filled annual CH₄ emissions were within their estimated uncertainty from each
639 other, apart from the year 2014. The results of different gap-filling methods were affected by the

640 different gap distributions and lengths in different years and the two wind sectors. Thus, below
641 we discuss the method performance separately for the year 2014 and the two other years.

642 The dataset from the eastern sector was gap-filled with higher confidence than for the western
643 sector in 2014. The data from the eastern sector contains fewer very long gaps - more than 30
644 days, and fewer long gaps - more than 8 but less than 30 days. The method which was most
645 affected by long gaps was the moving mean approach, indicating that this method should not be
646 used for data sets with very long gaps. The ANN and the GLM gap-filling methods based on the
647 whole data set estimated lower annual emission than mean emission from all methods. For two
648 years without very long gaps (2015 and 2016), the Jena gap-filling tool was assumed as a baseline
649 method, as it is commonly used for gap-filling of especially CO₂ fluxes. It is independent of the
650 user choices, as the ecosystem variables required have been chosen by the developers. However,
651 as this gap-filling tool has been developed for CO₂, not all the variables are necessarily relevant
652 for the gap-filling of the CH₄ time series. Furthermore, the Jena gap-filling tool works in a half-
653 hourly resolution to resolve the diel variation in CO₂ fluxes. As the sub-daily variation in CH₄ fluxes
654 is largely random noise in many mires (Rinne et al., 2007; 2018; Jackowicz-Korczyński et al., 2010),
655 developing a similar tool working at daily time step for CH₄, and with tailored parameter set for
656 CH₄, would be useful.

657 The moving mean approach resulted in annual fluxes within the range of standard deviation from
658 the Jena gap-filling tool. Daily values probably vary less than values obtained by the Jena tool
659 because moving means smooth the data. Additional advantages of this method are low input
660 requirements, as no auxiliary data is needed.

661 Annual estimates of CH₄ emission, based on the gap-filling with algorithms developed for the
662 whole data set, could be biased when the ecosystem is changing fast between the years and
663 functional dependencies on environmental parameters change. The annual CH₄ emissions by
664 ANN, based on the whole data set and based on one-year data, agree within the standard
665 deviation for the years 2015 and 2016. Both of them are also in agreement with the baseline
666 method within the standard deviation.

667 The feasibility of GLM is similar to ANN. The GLM model built on the whole dataset is sensitive to
668 rapid changes in ecosystem functioning and the number of gaps each year. A year with more gaps
669 has a lower influence on the model, similarly to the ANN. However, annual CH₄ emissions derived
670 using GLMs, based on each year separately or the whole dataset, agree with one another and
671 with baseline model within the standard deviation. GLM required more preparation than ANN.
672 Before developing the GLMs, highly correlated parameters need to be determined. The selection
673 of relevant variables is crucial for the correct performance of that algorithm and the selection
674 influences model output and model uncertainties.

675 According to the analysis with artificial gaps, the 35-day artificial gap did not change annual sums
676 significantly for any gap-filling method. The 80-day artificial gap created a significant difference
677 for the eastern sector in the year 2015 for ANN YbY and 2016 for ANN (Figure S7). The unfrozen

678 period did not show significant differences between annual sums for any method. The wintertime
679 period was statistically different for the year 2015 for ANN YbY. The results with the 80-day gap
680 had higher uncertainties than the results with a 35-day gap. The existence of gaps in the winter
681 period did not have a significant impact on the unfrozen period fluxes.

682 All presented methods show similar CH₄ emissions. Choosing one of them as the most
683 appropriate is not obvious, because all of them show both advantages and disadvantages. The
684 method that required the least amount of preparation before use and that was thus the fastest
685 to apply is the moving mean. It can be used for short gaps with good results and does not need
686 additional measured variables to work properly. The ANN method require less preparation than
687 other methods i.e. following the template or choosing the correct variables and it gives similar
688 results. It could be recommended as a gap-filling method suitable for different sites due to unique
689 construction of the ANN for each place.

690

691 4.3 Winter fluxes

692 The winter fluxes from both sectors were positive, which is in line with observations by e.g. Rinne
693 et al. (2007, 2018, 2020) and Jammet et al. (2017) of wintertime CH₄ emissions from frozen
694 northern mires. Winter emission and potential spring thaw bursts of CH₄ can be mechanistically
695 connected (Taylor et al. 2018), while degassing of CH₄ during the winter is likely to lead to smaller
696 or no thaw bursts of CH₄. Thus, EC studies on the seasonal cycle of CH₄ emissions from other
697 seasonally frozen mire ecosystems have shown minor or no thaw emission pulse (Rinne et al.,
698 2007; 2018; Mikhaylov et al. 2015). On the contrary, many studies show spring-thaw emissions
699 from shallow lakes (Raz-Yaseef et al. 2017, Jammet et al. 2015, 2017). In lakes, winter fluxes can
700 be blocked by a solid ice layer leading to the build-up of CH₄ below ice during the frozen period
701 (Jammet et al. 2017). On mires, however, the ice cover is not as solid as in lakes, but more porous
702 due to peat and plants within the ice. Therefore, the diffusion during the frozen period is
703 considerably faster than through lake ice. Furthermore, Song et al. (2012) showed that spring
704 burst events could occur at a very small scale and very short in duration (e.g. 2 hours). Small-scale
705 events show a lower influence on EC measurements because the method averages over a larger
706 area. Moreover, if the small-scale short-duration event does not happen in the EC footprint e.g.
707 due to wind direction, it will be missed.

708 We did not observe an autumn freeze-in burst in our data from either sector at Stordalen Mire.
709 These events have been observed at a High-Arctic tundra site (Mastepanov et al. 2013) though
710 not every year. Mastepanov et al. (2008) suggested that freeze-in bursts of CH₄ could be observed
711 only in the Arctic with continuous permafrost and not in a subarctic area with discontinuous or
712 sporadic permafrost. The phenomenon is assumed to be connected to the expansion of water
713 upon freezing, causing air bubbles to be mechanically pushed out of the freezing soil.

714

715 4.4 Different permafrost status and CH₄ emissions

716 Stordalen Mire is a complex mire system, with at least three different main wetlands surface
717 types and different permafrost status within a distance of a few hundred meters. The permafrost
718 palsa development and thaw depend both on temperature and snow cover and it is partly self-
719 regulating via the effect of microtopography on local snow depth (Johansson et al. 2006). Due to
720 the recently increasing temperatures, the thaw processes are currently likely to dominate over
721 palsa growth. CH₄ emission from the different microforms in mire systems depends on the
722 hydrological and nutrient status and temperature which affect e.g. plant and microbial
723 communities.

724 The carbon emitted as the CH₄ fluxes from the eastern and western sector is on similar level to
725 the Siikaneva fen (Rinne et al. 2018). In comparison to the other fen sites reviewed by Rinne et
726 al. (2018), the ratio of CH₄ to NEE at Stordalen Mire is higher. The reason behind this could be
727 the shorter growing season and thus lower CO₂ fluxes.

728 The average annual CH₄ emissions from different surfaces (Table 9) shows that the palsas have
729 the lowest annual CH₄ emissions, followed by a lake. The fully thawed fen, dominated by tall
730 graminoids, has very high annual CH₄ emissions and the highest of the mire complex, surpassing
731 e.g. many boreal poor fens (Nilsson et al., 2008; Rinne et al., 2018). The thawing surfaces common
732 in the eastern footprint of the tower have annual CH₄ emissions between palsas and tall sedge
733 fen. The three surface types studied here and previously by Jackowicz-Korczyński et al. (2010)
734 and Jammet et al., (2017) can be seen as forming a thaw gradient in this subarctic environment.
735 The globally rising temperature is likely to lead to continuing permafrost thaw in this kind of
736 ecosystem and increased CH₄ emissions.

737

738 5 Conclusion

739 At our study site, eddy covariance fluxes were measured for two different subarctic mire areas,
740 one dominated by palsa plateaus and the other a mixture of palsas and thawing wet surfaces.
741 The measurements revealed clear differences in their annual CH₄ emissions, with the area
742 dominated by palsas emitting less. The annual emission from a thawing surface (8.2 g-C m⁻² a⁻¹)
743 was nearly three times higher than from palsa surfaces (2.7 g-C m⁻² a⁻¹) but only half of the
744 emission previously reported from fully thawed tall graminoid fen. Areas measured in this study
745 had similar seasonal cycles of emission, with maxima appearing in August and lower but
746 significant fluxes in winter. The seasonal cycles were furthermore characterized by a fast increase
747 in spring (average 0.21 mg-C m⁻² d⁻² for the western sector and 0.68 mg-C m⁻² d⁻² for the eastern
748 sector) and a less rapid decrease in fall (average -0.16 mg-C m⁻² d⁻² for the western sector and -
749 0.37 mg-C m⁻² d⁻² for the eastern sector), without any obvious burst events during spring thaw or
750 autumn freeze-in. The wintertime period (from January to mid-May and from late-October to
751 December) contributed with 27 % - 45 % to the annual emission.

752 According to the correlation matrix and GLM analysis, CH₄ emissions from the western and
753 eastern sectors were partly controlled by different factors. As in most studies on CH₄ emission
754 from wetlands, peat temperature was the most important factor explaining the emission. The
755 relation of CH₄ flux with peat temperature at shallower depths showed similar hysteresis-like
756 behavior than observed by Chang et al. (2020), but inverse behavior with temperature at deeper
757 peat. We showed that the existence and direction of hysteresis-like behavior can depend on
758 which depth the temperature is measured.

759 The correlation of CH₄ emission and WTL in the eastern sector was not significant, but in the
760 western sector, the SWC did appear to control the emission.

761 The estimation of annual CH₄ emission was based on gap-filling with four different methods. All
762 methods resulted in similar annual fluxes, especially for the two years with just relatively short
763 gaps (less than 8 days). The performance of the methods was also dependent on the gap
764 distribution. Long gaps (more than 8 days) were the most problematic to be reconstructed by
765 any of the methods. The average annual emission from the western sector was 3.1 g-C m⁻² a⁻¹
766 and from the eastern sector was 5.5 g-C m⁻² a⁻¹. Both were substantially lower than those
767 obtained from a tall graminoid fen at the same mire system.

768 Based on the presented results further studies should focus on winter fluxes, which are important
769 in the northern, low emissions wetlands with discontinuous permafrost. There is still a lack in
770 understanding the processes behind those emissions. Also, the origin of wintertime CH₄ emission
771 is somewhat unknown. On the one hand, CH₄ can be produced during the winter period, on the
772 other hand CH₄ can also be produced during the growing season, remain stored in the peat and
773 then be slowly released during the frozen period. These processes could possibly explain the
774 hysteresis-like behavior of CH₄ emissions.

775

776 Data and code availability

777 <http://doi.org/10.5281/zenodo.4640164>

778

779 Author contribution

780 P.Ł., J.H. T.F., P.C. and J.R. analysed and interpreted the data. P.Ł., J.H., P.C., J.R. wrote the
781 manuscript. T.F., P.C. and, N.R. designed the measurements. N.K. was responsible for the
782 footprint calculation and its interpretation. P.-O.O. and L.E. were responsible for interpreting
783 UAV data. A. P. supported with the water table level data.

784

785 Competing interests

786 The authors declare that they have no conflict of interest

787

788 Acknowledgements

789 This study is funded by MEthane goes Mobile: MEasurement and MOdeling (MEMO2) project
790 from the European Union's Horizon 2020 research and innovation programme under the Marie
791 Sklodowska-Curie grant agreement No 722479. Data was provided by the Abisko Scientific
792 Research Station (ANS) and Swedish Infrastructure for Ecosystem Sciences (SITES, co-financed by
793 the Swedish Research Council) hosting the Stordalen site, part of the ICOS-Sweden network
794 which was co-financed by the Swedish Research Council (grant-no. 2015-06020, 2019-00205).
795 Image collection using the UAV was done by Matthias Siewert in collaboration with the SITES
796 Spectral project.

797 References

798 Åkerman, H. J. and Johansson, M.: Thawing permafrost and thicker active layers in sub-arctic
799 Sweden, *Permafr. Periglac. Process.*, 19, 279–292, <https://doi.org/10.1002/ppp.626>, 2008.

800 Bansal, S., Tangen, B., and Finocchiaro, R.: Temperature and Hydrology Affect Methane
801 Emissions from Prairie Pothole Wetlands, 36, 371–381, [https://doi.org/10.1007/s13157-016-](https://doi.org/10.1007/s13157-016-0826-8)
802 0826-8, 2016.

803 Brantley, H. L., Thoma, E. D., Squier, W. C., Guven, B. B., and Lyon, D.: Assessment of Methane
804 Emissions from Oil and Gas Production Pads using Mobile Measurements, *Environ. Sci.*
805 *Technol.*, 48, 14508–14515, <https://doi.org/10.1021/es503070q>, 2014.

806 Bubier, J., Moore, T., Savage, K., and Crill, P.: A comparison of methane flux in a boreal
807 landscape between a dry and a wet year, *Global Biogeochem. Cycles*, 19,
808 <https://doi.org/10.1029/2004GB002351>, 2005.

809 Budishchev, A., Mi, Y., van Huissteden, J., Belelli-Marchesini, L., Schaeppman-Strub, G.,
810 Parmentier, F. J. W., Fratini, G., Gallagher, A., Maximov, T. C., and Dolman, A. J.: Evaluation of a
811 plot-scale methane emission model using eddy covariance observations and footprint
812 modelling, 11, 4651–4664, <https://doi.org/10.5194/bg-11-4651-2014>, 2014.

813 Callaghan, T. V., Bergholm, F., Christensen, T. R., Jonasson, C., Kokfelt, U., and Johansson, M.: A
814 new climate era in the sub-Arctic: Accelerating climate changes and multiple impacts, *Geophys.*
815 *Res. Lett.*, 37, <https://doi.org/10.1029/2009GL042064>, 2010.

816 Callaghan, T. V., Jonasson, C., Thierfelder, T., Yang, Z., Hedenås, H., Johansson, M., Molau, U.,
817 Van Bogaert, R., Michelsen, A., Olofsson, J., Gwynn-Jones, D., Bokhorst, S., Phoenix, G., Bjerke,
818 J. W., Tømmervik, H., Christensen, T. R., Hanna, E., Koller, E. K., and Sloan, V. L.: Ecosystem
819 change and stability over multiple decades in the Swedish subarctic: complex processes and
820 multiple drivers, *Philos. Trans. R. Soc. B Biol. Sci.*, 368, 20120488,
821 <https://doi.org/10.1098/rstb.2012.0488>, 2013.

822 Chang, K.-Y., Riley, W. J., Crill, P. M., Grant, R. F., and Saleska, S. R.: Hysteretic temperature
823 sensitivity of wetland CH₄ fluxes explained by substrate availability and microbial activity, 17,
824 5849–5860, <https://doi.org/10.5194/bg-17-5849-2020>, 2020.

825 Christensen, T. R., Friborg, T., Sommerkorn, M., Kaplan, J., Illeris, L., Soegaard, H., Nordstroem,
826 C., and Jonasson, S.: Trace gas exchange in a high-Arctic valley: 1. Variations in CO₂ and CH₄ Flux
827 between tundra vegetation types, *Global Biogeochem. Cycles*, 14, 701–713,
828 <https://doi.org/10.1029/1999GB001134>, 2000.

829 Christensen, T. R., Ekberg, A., Ström, L., Mastepanov, M., Panikov, N., Öquist, M., Svensson, B.
830 H., Nykänen, H., Martikainen, P. J., and Oskarsson, H.: Factors controlling large scale variations
831 in methane emissions from wetlands, *Geophys. Res. Lett.*, 30,
832 <https://doi.org/10.1029/2002GL016848>, 2003.

833 Deng, J., Li, C., Frohking, S., Zhang, Y., Bäckstrand, K., and Crill, P.: Assessing effects of
834 permafrost thaw on C fluxes based on multiyear modeling across a permafrost thaw gradient at
835 Stordalen, Sweden, 11, 4753–4770, <https://doi.org/10.5194/bg-11-4753-2014>, 2014.

836 Dengel, S., Zona, D., Sachs, T., Aurela, M., Jammet, M., Parmentier, F. J. W., Oechel, W., and
837 Vesala, T.: Testing the applicability of neural networks as a gap-filling method using CH₄ flux
838 data from high latitude wetlands, 10, 8185–8200, <https://doi.org/10.5194/bg-10-8185-2013>,
839 2013.

840 Dlugokencky, E. J., Nisbet, E. G., Fisher, R., and Lowry, D.: Global atmospheric methane: budget,
841 changes and dangers, *Philos. Trans. R. Soc. A Math. Phys. Eng. Sci.*, 369, 2058–2072,
842 <https://doi.org/10.1098/rsta.2010.0341>, 2011.

843 Dobson 1945-, A. J.: An introduction to generalized linear models / Annette J. Dobson,
844 Chapman & Hall/CRC, Boca Raton, 2002.

845 Dragomir, C. M., Klaassen, W., Voiculescu, M., Georgescu, L. P., and van der Laan, S.: Estimating
846 Annual CO₂ Flux for Lutjewad Station Using Three Different Gap-Filling Techniques, *Sci. World*
847 *J.*, 2012, 842893, <https://doi.org/10.1100/2012/842893>, 2012.

848 Edie, R., Robertson, A. M., Field, R. A., Soltis, J., Snare, D. A., Zimmerle, D., Bell, C. S., Vaughn, T.
849 L., and Murphy, S. M.: Constraining the Accuracy of Flux Estimates Using OTM 33A, 2019, 1–27,
850 <https://doi.org/10.5194/amt-2019-306>, 2019.

851 Falge, E., Baldocchi, D., Olson, R., Anthoni, P., Aubinet, M., Bernhofer, C., Burba, G., Ceulemans,
852 R., Clement, R., Dolman, H., Granier, A., Gross, P., Grünwald, T., Hollinger, D., Jensen, N.-O.,
853 Katul, G., Keronen, P., Kowalski, A., Lai, C. T., Law, B. E., Meyers, T., Moncrieff, J., Moors, E.,
854 Munger, J. W., Pilegaard, K., Rannik, Ü., Rebmann, C., Suyker, A., Tenhunen, J., Tu, K., Verma, S.,
855 Vesala, T., Wilson, K., and Wofsy, S.: Gap filling strategies for defensible annual sums of net
856 ecosystem exchange, *Agric. For. Meteorol.*, 107, 43–69, [https://doi.org/10.1016/S0168-](https://doi.org/10.1016/S0168-1923(00)00225-2)
857 [1923\(00\)00225-2](https://doi.org/10.1016/S0168-1923(00)00225-2), 2001a.

858 Falge, E., Baldocchi, D., Olson, R., Anthoni, P., Aubinet, M., Bernhofer, C., Burba, G., Ceulemans,
859 R., Clement, R., Dolman, H. (A. J. ., Granier, A., Gross, P., Grünwald, T., Hollinger, D., Jensen, N.

860 O., Katul, G., Keronen, P., Kowalski, A., Lai, C.-T., and Tu, K.: Gap filling strategies for long term
861 energy flux data sets, *Agric. For. Meteorol.* 107 71-77, 2001b.

862 Fisher, R. E., France, J. L., Lowry, D., Lanoisellé, M., Brownlow, R., Pyle, J. A., Cain, M., Warwick,
863 N., Skiba, U. M., Drewer, J., Dinsmore, K. J., Leeson, S. R., Bauguitte, S. J.-B., Wellpott, A.,
864 O'Shea, S. J., Allen, G., Gallagher, M. W., Pitt, J., Percival, C. J., Bower, K., George, C., Hayman, G.
865 D., Aalto, T., Lohila, A., Aurela, M., Laurila, T., Crill, P. M., McCalley, C. K., and Nisbet, E. G.:
866 Measurement of the ¹³C isotopic signature of methane emissions from northern European
867 wetlands, *Global Biogeochem. Cycles*, 31, 605–623, <https://doi.org/10.1002/2016GB005504>,
868 2017.

869 Friborg, T., Christensen, T. R., and Sørensen, H.: Rapid response of greenhouse gas emission to
870 early spring thaw in a subarctic mire as shown by micrometeorological techniques, *Geophys.*
871 *Res. Lett.*, 24, 3061–3064, <https://doi.org/doi:10.1029/97GL03024>, 1997.

872 Gao, X., Adam Schlosser, C., Sokolov, A., Anthony, K. W., Zhuang, Q., and Kicklighter, D.:
873 Permafrost degradation and methane: low risk of biogeochemical climate-warming feedback,
874 *Environ. Res. Lett.*, 8, 35014, <https://doi.org/10.1088/1748-9326/8/3/035014>, 2013.

875 Gioli, B., Miglietta, F., Martino, B., Hutjes, R., Dolman, H. (A. J.), Lindroth, A., Schumacher, M.,
876 Sanz-Sanchez, M.-J., Manca, G., Peressotti, A., and Dumas, E.: Comparison between tower and
877 aircraft-based eddy covariance fluxes in five European regions, *Agric. For. Meteorol.*, 127, 1–16,
878 <https://doi.org/10.1016/j.agrformet.2004.08.004>, 2004.

879 Godin, A., McLaughlin, J. W., Webster, K. L., Packalen, M., and Basiliko, N.: Methane and
880 methanogen community dynamics across a boreal peatland nutrient gradient, *Soil Biol.*
881 *Biochem.*, 48, 96–105, <https://doi.org/https://doi.org/10.1016/j.soilbio.2012.01.018>, 2012.

882 Harenda, K., Lamentowicz, M., Samson, M., and Chojnicki, B.: The Role of Peatlands and Their
883 Carbon Storage Function in the Context of Climate Change, in: *GeoPlanet: Earth and Planetary*
884 *Sciences*, 169–187, https://doi.org/10.1007/978-3-319-71788-3_12, 2018.

885 Hommeltenberg, J., Schmid, H. P., Drösler, M., and Werle, P.: Can a bog drained for forestry be
886 a stronger carbon sink than a natural bog forest?, 11, 3477–3493, [https://doi.org/10.5194/bg-](https://doi.org/10.5194/bg-11-3477-2014)
887 11-3477-2014, 2014.

888 Intergovernmental Panel on Climate Change (Ed.): Anthropogenic and Natural Radiative
889 Forcing, in: *Climate Change 2013 – The Physical Science Basis: Working Group I Contribution to*
890 *the Fifth Assessment Report of the Intergovernmental Panel on Climate Change*, Cambridge
891 University Press, Cambridge, 659–740, [https://doi.org/DOI: 10.1017/CBO9781107415324.018](https://doi.org/DOI:10.1017/CBO9781107415324.018),
892 2014.

893 Ise, T., Dunn, A. L., Wofsy, S. C., and Moorcroft, P. R.: High sensitivity of peat decomposition to
894 climate change through water-table feedback, *Nat. Geosci.*, 1, 763–766,
895 <https://doi.org/10.1038/ngeo331>, 2008.

896 Jackowicz-Korczyński, M., Christensen, T. R., Bäckstrand, K., Crill, P., Friborg, T., Mastepanov,
897 M., and Ström, L.: Annual cycle of methane emission from a subarctic peatland, *J. Geophys. Res.*

898 Biogeosciences, 115, <https://doi.org/10.1029/2008JG000913>, 2010.

899 Jammet, M., Crill, P., Dengel, S., and Friborg, T.: Large methane emissions from a subarctic lake
900 during spring thaw: Mechanisms and landscape significance, *J. Geophys. Res. Biogeosciences*,
901 120, 2289–2305, <https://doi.org/10.1002/2015JG003137>, 2015.

902 Jammet, M., Dengel, S., Kettner, E., Parmentier, F.-J. W., Wik, M., Crill, P., and Friborg, T.: Year-
903 round CH₄ and CO₂ flux dynamics in two contrasting freshwater ecosystems of the subarctic,
904 14, 5189–5216, <https://doi.org/10.5194/bg-14-5189-2017>, 2017.

905 JOHANSSON, T., MALMER, N., CRILL, P. M., FRIBORG, T., ÅKERMAN, J. H., MASTEPANOV, M.,
906 and CHRISTENSEN, T. R.: Decadal vegetation changes in a northern peatland, greenhouse gas
907 fluxes and net radiative forcing, *Glob. Chang. Biol.*, 12, 2352–2369,
908 <https://doi.org/10.1111/j.1365-2486.2006.01267.x>, 2006.

909 Kirschke, S., Bousquet, P., Ciais, P., Saunois, M., Canadell, J. G., Dlugokencky, E. J., Bergamaschi,
910 P., Bergmann, D., Blake, D. R., Bruhwiler, L., Cameron-Smith, P., Castaldi, S., Chevallier, F., Feng,
911 L., Fraser, A., Heimann, M., Hodson, E. L., Houweling, S., Josse, B., Fraser, P. J., Krummel, P. B.,
912 Lamarque, J.-F., Langenfelds, R. L., Le Quéré, C., Naik, V., O’Doherty, S., Palmer, P. I., Pison, I.,
913 Plummer, D., Poulter, B., Prinn, R. G., Rigby, M., Ringeval, B., Santini, M., Schmidt, M., Shindell,
914 D. T., Simpson, I. J., Spahni, R., Steele, L. P., Strode, S. A., Sudo, K., Szopa, S., van der Werf, G. R.,
915 Voulgarakis, A., van Weele, M., Weiss, R. F., Williams, J. E., and Zeng, G.: Three decades of
916 global methane sources and sinks, *Nat. Geosci.*, 6, 813–823, <https://doi.org/10.1038/ngeo1955>,
917 2013.

918 Kljun, N., Calanca, P., Rotach, M. W., and Schmid, H. P.: A simple two-dimensional
919 parameterisation for Flux Footprint Prediction (FFP), *Geosci. Model Dev.*, 8, 3695–3713,
920 <https://doi.org/10.5194/gmd-8-3695-2015>, 2015.

921 Knox, S. H., Matthes, J. H., Sturtevant, C., Oikawa, P. Y., Verfaillie, J., and Baldocchi, D.:
922 Biophysical controls on interannual variability in ecosystem-scale CO₂ and CH₄ exchange in a
923 California rice paddy, *J. Geophys. Res. Biogeosciences*, 121, 978–1001,
924 <https://doi.org/10.1002/2015JG003247>, 2016.

925 Knox, S. H., Windham-Myers, L., Anderson, F., Sturtevant, C., and Bergamaschi, B.: Direct and
926 Indirect Effects of Tides on Ecosystem-Scale CO₂ Exchange in a Brackish Tidal Marsh in Northern
927 California, *J. Geophys. Res. Biogeosciences*, 123, 787–806,
928 <https://doi.org/10.1002/2017JG004048>, 2018.

929 Kowalska, N., Chojnicki, B., Rinne, J., Haapanala, S., Siedlecki, P., Urbaniak, M., Juszczak, R., and
930 Olejnik, J.: Measurements of methane emission from a temperate wetland by eddy covariance
931 method, *Int. Agrophysics*, 27, 283–290, <https://doi.org/10.2478/v10247-012-0096-5>, 2013.

932 LEVENBERG, K.: A METHOD FOR THE SOLUTION OF CERTAIN NON-LINEAR PROBLEMS IN LEAST
933 SQUARES, *Q. Appl. Math.*, 2, 164–168, 1944.

934 Li, T., Raivonen, M., Alekseychik, P., Aurela, M., Lohila, A., Zheng, X., Zhang, Q., Wang, G.,
935 Mammarella, I., Rinne, J., Yu, L., Xie, B., Vesala, T., and Zhang, W.: Importance of vegetation

936 classes in modeling CH₄ emissions from boreal and subarctic wetlands in Finland, *Sci. Total*
937 *Environ.*, 572, 1111–1122, [https://doi.org/https://doi.org/10.1016/j.scitotenv.2016.08.020](https://doi.org/10.1016/j.scitotenv.2016.08.020),
938 2016.

939 LUNDEGÅRDH, H.: CARBON DIOXIDE EVOLUTION OF SOIL AND CROP GROWTH, *Soil Sci.*, 23,
940 1927.

941 Malmer, N., Johansson, T., Olsrud, M., and Christensen, T. R.: Vegetation, climatic changes and
942 net carbon sequestration in a North-Scandinavian subarctic mire over 30 years, *Glob. Chang.*
943 *Biol.*, 11, 1895–1909, <https://doi.org/10.1111/j.1365-2486.2005.01042.x>, 2005.

944 Marquardt, D. W.: An Algorithm for Least-Squares Estimation of Nonlinear Parameters, *J. Soc.*
945 *Ind. Appl. Math.*, 11, 431–441, 1963.

946 Mastepanov, M., Sigsgaard, C., Dlugokencky, E. J., Houweling, S., Ström, L., Tamstorf, M. P., and
947 Christensen, T. R.: Large tundra methane burst during onset of freezing, *Nature*, 456, 628–630,
948 <https://doi.org/10.1038/nature07464>, 2008.

949 Mastepanov, M., Sigsgaard, C., Tagesson, T., Ström, L., Tamstorf, M. P., Lund, M., and
950 Christensen, T. R.: Revisiting factors controlling methane emissions from high-Arctic tundra, 10,
951 5139–5158, <https://doi.org/10.5194/bg-10-5139-2013>, 2013.

952 Mauder, M. and Foken, T.: Documentation and Instruction Manual of the Eddy Covariance
953 Software Package TK2, Arbeitsergebnisse, Univ. Bayreuth, Abteilung Mikrometeorologie, ISSN
954 1614-8916, 46, <https://doi.org/10.5194/bg-5-451-2008>, 2011.

955 McCalley, C. K., Woodcroft, B. J., Hodgkins, S. B., Wehr, R. A., Kim, E.-H., Mondav, R., Crill, P. M.,
956 Chanton, J. P., Rich, V. I., Tyson, G. W., and Saleska, S. R.: Methane dynamics regulated by
957 microbial community response to permafrost thaw, *Nature*, 514, 478–481,
958 <https://doi.org/10.1038/nature13798>, 2014.

959 McGuire, A. D., Christensen, T. R., Hayes, D., Heroult, A., Euskirchen, E., Kimball, J. S., Koven, C.,
960 Lafleur, P., Miller, P. A., Oechel, W., Peylin, P., Williams, M., and Yi, Y.: An assessment of the
961 carbon balance of Arctic tundra: comparisons among observations, process models, and
962 atmospheric inversions, 9, 3185–3204, <https://doi.org/10.5194/bg-9-3185-2012>, 2012.

963 Melloh, R. A. and Crill, P. M.: Winter methane dynamics in a temperate peatland, *Global*
964 *Biogeochem. Cycles*, 10, 247–254, <https://doi.org/doi:10.1029/96GB00365>, 1996.

965 Mikhaylov, O. A., Miglovets, M. N., and Zagirova, S. V.: Vertical methane fluxes in
966 mesooligotrophic boreal peatland in European Northeast Russia, *Contemp. Probl. Ecol.*, 8, 368–
967 375, <https://doi.org/10.1134/S1995425515030099>, 2015.

968 Moorcroft, P., Wofsy, S., Dunn, A., and Ise, T.: High sensitivity of peat decomposition to climate
969 change through water-table feedback, *Nat. Geosci.*, 1, <https://doi.org/10.1038/ngeo331>, 2008.

970 Natali, S. M., Watts, J. D., Rogers, B. M., Potter, S., Ludwig, S. M., Selbmann, A.-K., Sullivan, P. F.,
971 Abbott, B. W., Arndt, K. A., Birch, L., Björkman, M. P., Bloom, A. A., Celis, G., Christensen, T. R.,
972 Christiansen, C. T., Commane, R., Cooper, E. J., Crill, P., Czimczik, C., Davydov, S., Du, J., Egan, J.

973 E., Elberling, B., Euskirchen, E. S., Friborg, T., Genet, H., Göckede, M., Goodrich, J. P., Grogan, P.,
974 Helbig, M., Jafarov, E. E., Jastrow, J. D., Kalhori, A. A. M., Kim, Y., Kimball, J. S., Kutzbach, L.,
975 Lara, M. J., Larsen, K. S., Lee, B.-Y., Liu, Z., Lorant, M. M., Lund, M., Lupascu, M., Madani, N.,
976 Malhotra, A., Matamala, R., McFarland, J., McGuire, A. D., Michelsen, A., Minions, C., Oechel,
977 W. C., Olefeldt, D., Parmentier, F.-J. W., Pirk, N., Poulter, B., Quinton, W., Rezanezhad, F., Risk,
978 D., Sachs, T., Schaefer, K., Schmidt, N. M., Schuur, E. A. G., Semenchuk, P. R., Shaver, G.,
979 Sonnentag, O., Starr, G., Treat, C. C., Waldrop, M. P., Wang, Y., Welker, J., Wille, C., Xu, X.,
980 Zhang, Z., Zhuang, Q., and Zona, D.: Large loss of CO₂ in winter observed across the northern
981 permafrost region, *Nat. Clim. Chang.*, 9, 852–857, <https://doi.org/10.1038/s41558-019-0592-8>,
982 2019.

983 Nemitz, E., Mammarella, I., Ibrom, A., Aurela, M., Burba, G., Dengel, S., Gielen, B., Grelle, A.,
984 Heinesch, B., Herbst, M., Hörtnagl, L., Klemetsson, L., Lindroth, A., Lohila, A., Mcdermitt, D.,
985 Meier, P., Merbold, L., Nelson, D., Nicolini, G., and Zahniser, M.: Standardisation of eddy-
986 covariance flux measurements of methane and nitrous oxide, *Int. Agrophysics*, 32, 517–549,
987 <https://doi.org/10.1515/intag-2017-0042>, 2018.

988 NILSSON, M., SAGERFORS, J., BUFFAM, I., LAUDON, H., ERIKSSON, T., GRELE, A.,
989 KLEMEDTSSON, L., WESLIEN, P. E. R., and LINDROTH, A.: Contemporary carbon accumulation in
990 a boreal oligotrophic minerogenic mire – a significant sink after accounting for all C-fluxes,
991 *Glob. Chang. Biol.*, 14, 2317–2332, <https://doi.org/10.1111/j.1365-2486.2008.01654.x>, 2008.

992 Nisbet, E. G., Dlugokencky, E. J., and Bousquet, P.: Methane on the Rise—Again, *Science (80-.)*,
993 343, 493 LP – 495, <https://doi.org/10.1126/science.1247828>, 2014.

994 Nisbet, E. G., Dlugokencky, E. J., Manning, M. R., Lowry, D., Fisher, R. E., France, J. L., Michel, S.
995 E., Miller, J. B., White, J. W. C., Vaughn, B., Bousquet, P., Pyle, J. A., Warwick, N. J., Cain, M.,
996 Brownlow, R., Zazzeri, G., Lanoisellé, M., Manning, A. C., Gloor, E., Worthy, D. E. J., Brunke, E.-
997 G., Labuschagne, C., Wolff, E. W., and Ganesan, A. L.: Rising atmospheric methane: 2007–2014
998 growth and isotopic shift, *Global Biogeochem. Cycles*, 30, 1356–1370,
999 <https://doi.org/10.1002/2016GB005406>, 2016.

1000 of Sciences Engineering and Medicine: Improving Characterization of Anthropogenic Methane
1001 Emissions in the United States, The National Academies Press, Washington, DC,
1002 <https://doi.org/10.17226/24987>, 2018.

1003 Olefeldt, D., Roulet, N. T., Bergeron, O., Crill, P., Bäckstrand, K., and Christensen, T. R.: Net
1004 carbon accumulation of a high-latitude permafrost tundra mire similar to permafrost-free
1005 peatlands, *Geophys. Res. Lett.*, 39, <https://doi.org/10.1029/2011GL050355>, 2012.

1006 Parmentier, F. J. W., van Huissteden, J., van der Molen, M. K., Schaepman-Strub, G., Karsanaev,
1007 S. A., Maximov, T. C., and Dolman, A. J.: Spatial and temporal dynamics in eddy covariance
1008 observations of methane fluxes at a tundra site in northeastern Siberia, *J. Geophys. Res.*
1009 *Biogeosciences*, 116, <https://doi.org/10.1029/2010JG001637>, 2011.

1010 Post, E., Alley, R. B., Christensen, T. R., Macias-Fauria, M., Forbes, B. C., Gooseff, M. N., Iler, A.,
1011 Kerby, J. T., Laidre, K. L., Mann, M. E., Olofsson, J., Stroeve, J. C., Ulmer, F., Virginia, R. A., and

1012 Wang, M.: The polar regions in a 2^{\textdegree}C warmer world, *Sci. Adv.*, 5,
1013 <https://doi.org/10.1126/sciadv.aaw9883>, 2019.

1014 Pugh, C. A., Reed, D. E., Desai, A. R., and Sulman, B. N.: Wetland flux controls: how does
1015 interacting water table levels and temperature influence carbon dioxide and methane fluxes in
1016 northern Wisconsin?, *Biogeochemistry*, 137, 15–25, [https://doi.org/10.1007/s10533-017-0414-](https://doi.org/10.1007/s10533-017-0414-x)
1017 [x](https://doi.org/10.1007/s10533-017-0414-x), 2018.

1018 Raz-Yaseef, N., Torn, M. S., Wu, Y., Billesbach, D. P., Liljedahl, A. K., Kneafsey, T. J., Romanovsky,
1019 V. E., Cook, D. R., and Wullschleger, S. D.: Large CO₂ and CH₄ emissions from polygonal tundra
1020 during spring thaw in northern Alaska, *Geophys. Res. Lett.*, 44, 504–513,
1021 <https://doi.org/10.1002/2016GL071220>, 2017.

1022 Rebmann, C., Aubinet, M., Schmid, H., Arriga, N., Aurela, M., Burba, G., Clement, R., De Ligne,
1023 A., Fratini, G., Gielen, B., Grace, J., Graf, A., Gross, P., Haapanala, S., Herbst, M., Hörtnagl, L.,
1024 Ibrom, A., Joly, L., Kljun, N., and Franz, D.: ICOS eddy covariance flux-station site setup: A
1025 review, *Int. Agrophysics*, 32, 471–494, <https://doi.org/10.1515/intag-2017-0044>, 2018.

1026 Rindskopf, D.: Generalized linear models., <https://doi.org/10.1037/13621-009>, 2012.

1027 Rinne, J., Riutta, T., Pihlatie, M., Aurela, M., Haapanala, S., Tuovinen, J.-P., Tuittila, E.-S., and
1028 Vesala, T.: Annual cycle of methane emission from a boreal fen measured by the eddy
1029 covariance technique, *Tellus B Chem. Phys. Meteorol.*, 59, 449–457,
1030 <https://doi.org/10.1111/j.1600-0889.2007.00261.x>, 2007.

1031 Rinne, J., Tuittila, E.-S., Peltola, O., Li, X., Raivonen, M., Alekseychik, P., Haapanala, S., Pihlatie,
1032 M., Aurela, M., Mammarella, I., and Vesala, T.: Temporal Variation of Ecosystem Scale Methane
1033 Emission From a Boreal Fen in Relation to Temperature, Water Table Position, and Carbon
1034 Dioxide Fluxes, *Global Biogeochem. Cycles*, 32, 1087–1106,
1035 <https://doi.org/10.1029/2017GB005747>, 2018.

1036 Rinne, J., Tuovinen, J.-P., Klemetsson, L., Aurela, M., Holst, J., Lohila, A., Weslien, P., Vestin, P.,
1037 Łakomiec, P., Peichl, M., Tuittila, E.-S., Heiskanen, L., Laurila, T., Li, X., Alekseychik, P.,
1038 Mammarella, I., Ström, L., Crill, P., and Nilsson, M. B.: Effect of the 2018 European drought on
1039 methane and carbon dioxide exchange of northern mire ecosystems, *Philos. Trans. R. Soc. B*
1040 *Biol. Sci.*, 375, 20190517, <https://doi.org/10.1098/rstb.2019.0517>, 2020.

1041 Robertson, A. M., Edie, R., Snare, D., Soltis, J., Field, R. A., Burkhart, M. D., Bell, C. S., Zimmerle,
1042 D., and Murphy, S. M.: Variation in Methane Emission Rates from Well Pads in Four Oil and Gas
1043 Basins with Contrasting Production Volumes and Compositions, *Environ. Sci. Technol.*, 51,
1044 8832–8840, <https://doi.org/10.1021/acs.est.7b00571>, 2017.

1045 Röckmann, T., Eyer, S., Veen, C., Popa, E., Tuzson, B., Monteil, G., Houweling, S., Harris, E.,
1046 Brunner, D., Fischer, H., Zazzeri, G., Lowry, D., Nisbet, E., Brand, W., Necki, J., Emmenegger, L.,
1047 and Mohn, J.: In situ observations of the isotopic composition of methane at the Cabauw tall
1048 tower site, *Atmos. Chem. Phys.*, 16, 10469–10487, <https://doi.org/10.5194/acp-16-10469-2016>,
1049 2016.

- 1050 Rößger, N., Wille, C., Holl, D., Göckede, M., and Kutzbach, L.: Scaling and balancing carbon
1051 dioxide fluxes in a heterogeneous tundra ecosystem of the Lena River Delta, 16, 2591–2615,
1052 <https://doi.org/10.5194/bg-16-2591-2019>, 2019.
- 1053 Saunio, M., Bousquet, P., Poulter, B., Peregón, A., Ciais, P., Canadell, J. G., Dlugokencky, E. J.,
1054 Etiope, G., Bastviken, D., Houweling, S., Janssens-Maenhout, G., Tubiello, F. N., Castaldi, S.,
1055 Jackson, R. B., Alexe, M., Arora, V. K., Beerling, D. J., Bergamaschi, P., Blake, D. R., Brailsford, G.,
1056 Brovkin, V., Bruhwiler, L., Crevoisier, C., Crill, P., Covey, K., Curry, C., Frankenberg, C., Gedney,
1057 N., Höglund-Isaksson, L., Ishizawa, M., Ito, A., Joos, F., Kim, H.-S., Kleinen, T., Krummel, P.,
1058 Lamarque, J.-F., Langenfelds, R., Locatelli, R., Machida, T., Maksyutov, S., McDonald, K. C.,
1059 Marshall, J., Melton, J. R., Morino, I., Naik, V., O’Doherty, S., Parmentier, F.-J. W., Patra, P. K.,
1060 Peng, C., Peng, S., Peters, G. P., Pison, I., Prigent, C., Prinn, R., Ramonet, M., Riley, W. J., Saito,
1061 M., Santini, M., Schroeder, R., Simpson, I. J., Spahni, R., Steele, P., Takizawa, A., Thornton, B. F.,
1062 Tian, H., Tohjima, Y., Viovy, N., Voulgarakis, A., van Weele, M., van der Werf, G. R., Weiss, R.,
1063 Wiedinmyer, C., Wilton, D. J., Wiltshire, A., Worthy, D., Wunch, D., Xu, X., Yoshida, Y., Zhang, B.,
1064 Zhang, Z., and Zhu, Q.: The global methane budget 2000–2012, *Earth Syst. Sci. Data*, 8, 697–
1065 751, <https://doi.org/10.5194/essd-8-697-2016>, 2016.
- 1066 Saunio, M., Stavert, A. R., Poulter, B., Bousquet, P., Canadell, J. G., Jackson, R. B., Raymond, P.
1067 A., Dlugokencky, E. J., Houweling, S., Patra, P. K., Ciais, P., Arora, V. K., Bastviken, D.,
1068 Bergamaschi, P., Blake, D. R., Brailsford, G., Bruhwiler, L., Carlson, K. M., Carrol, M., Castaldi, S.,
1069 Chandra, N., Crevoisier, C., Crill, P. M., Covey, K., Curry, C. L., Etiope, G., Frankenberg, C.,
1070 Gedney, N., Hegglin, M. I., Höglund-Isaksson, L., Hugelius, G., Ishizawa, M., Ito, A., Janssens-
1071 Maenhout, G., Jensen, K. M., Joos, F., Kleinen, T., Krummel, P. B., Langenfelds, R. L., Laruelle, G.
1072 G., Liu, L., Machida, T., Maksyutov, S., McDonald, K. C., McNorton, J., Miller, P. A., Melton, J. R.,
1073 Morino, I., Müller, J., Murguia-Flores, F., Naik, V., Niwa, Y., Noce, S., O’Doherty, S., Parker, R. J.,
1074 Peng, C., Peng, S., Peters, G. P., Prigent, C., Prinn, R., Ramonet, M., Regnier, P., Riley, W. J.,
1075 Rosentreter, J. A., Segers, A., Simpson, I. J., Shi, H., Smith, S. J., Steele, L. P., Thornton, B. F.,
1076 Tian, H., Tohjima, Y., Tubiello, F. N., Tsuruta, A., Viovy, N., Voulgarakis, A., Weber, T. S., van
1077 Weele, M., van der Werf, G. R., Weiss, R. F., Worthy, D., Wunch, D., Yin, Y., Yoshida, Y., Zhang,
1078 W., Zhang, Z., Zhao, Y., Zheng, B., Zhu, Q., Zhu, Q., and Zhuang, Q.: The Global Methane Budget
1079 2000–2017, *Earth Syst. Sci. Data*, 12, 1561–1623, <https://doi.org/10.5194/essd-12-1561-2020>,
1080 2020.
- 1081 Song, C., Xu, X., Sun, X., Tian, H., Sun, L., Miao, Y., Wang, X., and Guo, Y.: Large methane
1082 emission upon spring thaw from natural wetlands in the northern permafrost region, *Environ.*
1083 *Res. Lett.*, 7, 034009, <https://doi.org/10.1088/1748-9326/7/3/034009>, 2012.
- 1084 Sturtevant, C. S., Oechel, W. C., Zona, D., Kim, Y., and Emerson, C. E.: Soil moisture control over
1085 autumn season methane flux, Arctic Coastal Plain of Alaska, 9, 1423–1440,
1086 <https://doi.org/10.5194/bg-9-1423-2012>, 2012.
- 1087 T, V., Eugster, W., and Ojala, A.: Eddy Covariance: A Practical Guide to Measurement and Data
1088 Analysis, in: Springer Atmospheric Sciences Series, vol. 12, 365–376,
1089 <https://doi.org/10.1007/978-94-007-2351-1>, 2012.

1090 Taylor, M. A., Celis, G., Ledman, J. D., Bracho, R., and Schuur, E. A. G.: Methane Efflux Measured
1091 by Eddy Covariance in Alaskan Upland Tundra Undergoing Permafrost Degradation, *J. Geophys.*
1092 *Res. Biogeosciences*, 123, 2695–2710, <https://doi.org/10.1029/2018JG004444>, 2018.

1093 Turetsky, M. R., Kotowska, A., Bubier, J., Dise, N. B., Crill, P., Hornibrook, E. R. C., Minkinen, K.,
1094 Moore, T. R., Myers-Smith, I. H., Nykänen, H., Olefeldt, D., Rinne, J., Saarnio, S., Shurpali, N.,
1095 Tuittila, E.-S., Waddington, J. M., White, J. R., Wickland, K. P., and Wilmking, M.: A synthesis of
1096 methane emissions from 71 northern, temperate, and subtropical wetlands, *Glob. Chang. Biol.*,
1097 20, 2183–2197, <https://doi.org/10.1111/gcb.12580>, 2014.

1098 Vellinga, O. S., Dobosy, R. J., Dumas, E. J., Gioli, B., Elbers, J. A., and Hutjes, R. W. A.: Calibration
1099 and Quality Assurance of Flux Observations from a Small Research Aircraft*, *J. Atmos. Ocean.*
1100 *Technol.*, 30, 161–181, <https://doi.org/10.1175/JTECH-D-11-00138.1>, 2013.

1101 Verma, S. B., Baldocchi, D. D., Anderson, D. E., Matt, D. R., and Clement, R. J.: Eddy fluxes of
1102 CO₂, water vapor, and sensible heat over a deciduous forest, *Boundary-Layer Meteorol.*, 36,
1103 71–91, <https://doi.org/10.1007/BF00117459>, 1986.

1104 Woodcroft, B. J., Singleton, C. M., Boyd, J. A., Evans, P. N., Emerson, J. B., Zayed, A. A. F.,
1105 Hoelzle, R. D., Lamberton, T. O., McCalley, C. K., Hodgkins, S. B., Wilson, R. M., Purvine, S. O.,
1106 Nicora, C. D., Li, C., Frohling, S., Chanton, J. P., Crill, P. M., Saleska, S. R., Rich, V. I., and Tyson, G.
1107 W.: Genome-centric view of carbon processing in thawing permafrost, *Nature*, 560, 49–54,
1108 <https://doi.org/10.1038/s41586-018-0338-1>, 2018.

1109 Wutzler, T., Lucas-Moffat, A., Migliavacca, M., Knauer, J., Sickel, K., Šigut, L., Menzer, O., and
1110 Reichstein, M.: Basic and extensible post-processing of eddy covariance flux data with
1111 REddyProc, 15, 5015–5030, <https://doi.org/10.5194/bg-15-5015-2018>, 2018.

1112 Yamulki, S., Anderson, R., Peace, A., and Morison, J. I. L.: Soil CO₂, CH₄ and N₂O
1113 fluxes from an afforested lowland raised peatbog in Scotland: implications for drainage and
1114 restoration, 10, 1051–1065, <https://doi.org/10.5194/bg-10-1051-2013>, 2013.

1115 Zhang, Z., Zimmermann, N. E., Stenke, A., Li, X., Hodson, E. L., Zhu, G., Huang, C., and Poulter,
1116 B.: Emerging role of wetland methane emissions in driving 21st century climate change, *Proc.*
1117 *Natl. Acad. Sci.*, 114, 9647–9652, <https://doi.org/10.1073/pnas.1618765114>, 2017.

1118